esa SCI(97)2
October 1997

VERY LOW FREQUENCY ARRAY ON THE LUNAR FAR SIDE

Report by the
Very Low Frequency Astronomy Study Team

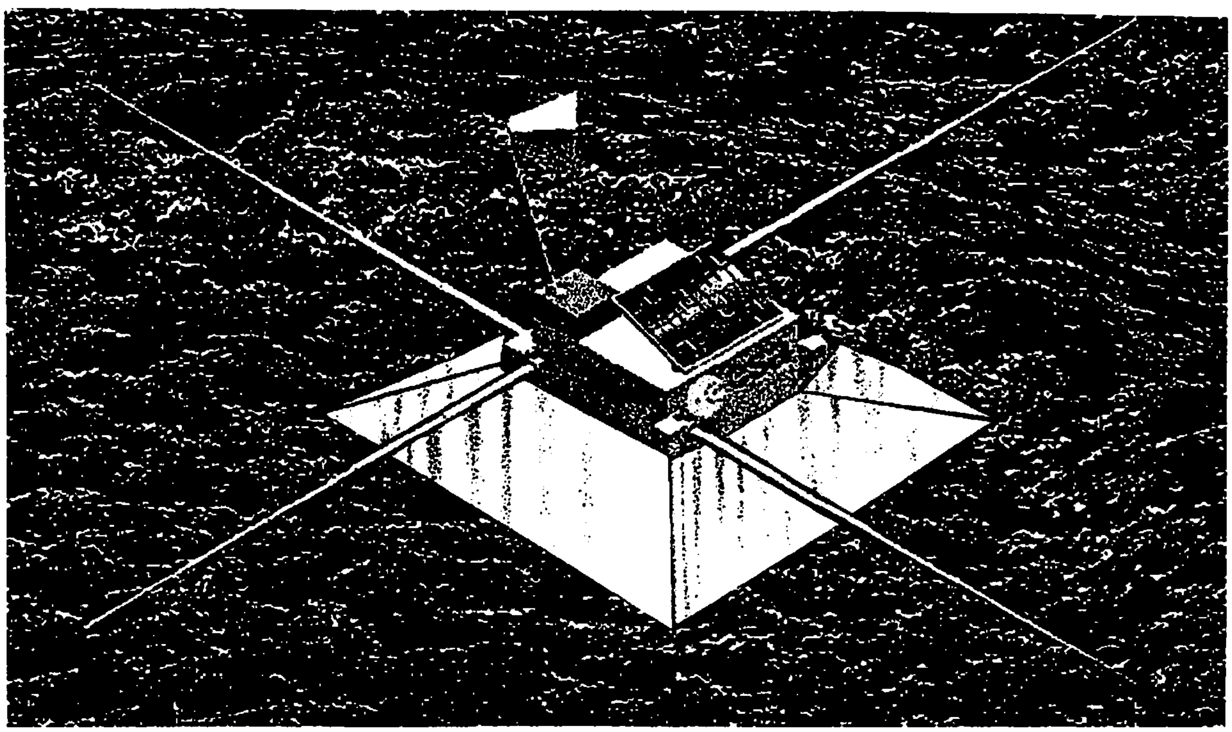

european space agency
agence spatiale européenne

8-10 rue Mario Nikis 75738 Paris Cedex 15, France

esa

esa SCI(97)2
October 1997

VERY LOW FREQUENCY ARRAY ON THE LUNAR FAR SIDE

Report by the
Very Low Frequency Astronomy Study Team

european space agency
agence spatiale européenne

8-10 rue Mario Nikis 75738 Paris Cedex 15, France

TABLE OF CONTENTS

Executive Summary 1
Foreword 2
1. Introduction 3
2 Science Program 5
2.1 Introduction to VLF radio astronomy 5
2.2 The Universe at low radio frequencies 9
2.3 Solar system 13
3 Why the lunar far side? 19
4 Design considerations 21
4.1 Scattering effects in turbulent plasmas 21
4.2 Absorption effects 28
4.3 Investigating the interstellar medium 29
4.4 Electrical properties of the Moon 31
4.5 Telescope design for an all-sky survey 34
4.6 Overall summary 41
5 Baseline specifications 45
5.1 All sky survey 45
5.1 Solar system receiver requirements 46
6 A strawman design 47
6.1 Array configuration 47
6.2 Spiral configuration 48
6.3 Data processing and communication 51
6.4 Receiver elements 52
6.5 Solar system receiver 57
6.6 Central station 57
6.7 Site selection 58
7 Launch and deployment 61
8 Cost estimate 63
9 Precursor mission 65
10 Conclusion 67
Appendix A Study participants 68

EXECUTIVE SUMMARY

The radio region below 20 MHz is the last unexplored window of the electromagnetic spectrum. Far from showing a simple extension of more energetic phenomena, very low frequencies promise new insights in the physics of supernova remnants, the interstellar medium, cosmic rays, quasars and radiogalaxies.

The Earth's natural ionosphere prevents all but the most crude measurements from the ground and the near-earth environment is now so polluted by man-made radio interference that sensitive observations are impossible, even from earth-orbiting satellites.

Within our solar system, the far side of the Moon offers unique advantages for performing radio astronomy at very low frequencies. It is well shielded from man-made and natural interference from the Earth and its ionosphere is very thin, especially during the lunar night. It is relatively close to the earth and is a stable platform on which a large array can be deployed.

The instrument that we propose is an array of 300 independent receiving elements arranged in a spiralled-'Y' within an enclosing circle 40 km in diameter. This array is designed to perform all-sky surveys within the frequency range of 0.5 to 16 MHz with an angular resolution of at least 0.5 degrees. The sensitivity is sufficient to map the sky down to the confusion limit imposed by the galactic background. The instrument is also capable of performing directed observations of specific sources, within the solar system, on time scales down to those imposed by the interplanetary scattering limit.

The mission can be completed within 5 years, with observations carried out mostly during the lunar night so as to avoid solar interference and effects from the Moon's ionosphere. Each survey, covering a bandwidth of 100 kHz, is completed within a lunar night by 'Moon rotation synthesis'.

The individual receivers are composed of two 4-meter long crossed dipoles mounted on a small box containing the receiver electronics. The data are transmitted to a central station, via repeaters for the most distant receivers. During lunar night, when observations are carried out, power is supplied by an ultra-lightweight battery charged during the lunar day by a small solar array.

Correlation is performed in the central station to reduce the volume of data to be transmitted back to Earth. The data are relayed to earth via a satellite on a halo orbit around the second Lagrange point of the earth-moon system, with continuous visibility of both the earth and the central station.

The 300 elements and central station, with a total weight on the order of 1250 kg, are delivered to the moon's surface in a single Ariane 5 launch. Deployment of the elements is performed robotically using a rover reassigned from the moon exploration program.

This study has confirmed the exciting possibilities of very low frequency radio astronomy and showed the feasibility of the project within the framework of Phase III of the ESA Moon program: "science from the moon". Before the mission can be started, however, a number of in-situ measurements need to be performed to confirm certain environmental conditions. We recommend continuing the study of the concept proposed here and the inclusion of a dedicated measurement program in the MORO and LEDA missions.

FOREWORD

In its report to ESA *Mission to the Moon*, the Lunar Steering Group identified very-low-frequency astronomy as a promising observation science which could benefit from the installation of a low-frequency radio telescope array on the far side of the moon. In the following study phase devoted to the definition of a European view of Lunar exploration and exploitation, a Very Low Frequency (VLF) group was set up in September 1993. The group was charged with the task of identifying the prime scientific objectives of a very-low-frequency observatory and establishing the case for its being lunar based.

Following the recommendations of the VLF group, ESA decided to conduct a preliminary design study of a moon-based very low frequency array. This study was contracted out to CASA of Madrid with a subcontractor, DETyCOM, working in the antenna and radio frequency field. The study was initiated in February 1995 and ran for one year. The work was performed under the guidance of the Very Low Frequency Astronomy Study Team.

During the course of the study, the team took a detailed look at the practical observing limitations in the frequency band below 10 MHz due to interplanetary and interstellar scattering. From these limitations on spatial and temporal resolution, scientific objectives were established from which a set of requirements could be produced for the array. From these deliberations the study team concluded that the observatory should consist of an instrument capable of performing an all sky survey supplemented by an instrument optimised for solar system observations.

The present report summarises the reflections of the Study Team and the results of the technical study performed by CASA and their subcontractor DETyCOM. Technical details and supporting design documents can be found in the engineering notes of CASA.

The ESA Directorate of Scientific Programme staff responsible for the study were:

Pierre-Yves Bély	Study Scientist, Chairman
R. J. Laurance	Study Manager
S. Volonte	Astronomy Missions Coordinator

The external experts members of the Space Interferometry Study Team were:

Roberto R. Ambrosini	Istituto di Radioastronomia Bologna (Italy)
Arnold van Ardenne	NFRA Dwingeloo (NL)
Colin H. Barrow	Max-Planck-Institut für Aeronomie (Germany)
Jean-Louis Bougeret	Observatoire de Paris-Meudon (France)
Juan-Maria Marcaide	Universidad de Valencia (Spain)
Graham Woan	Cavendish Laboratory, Cambridge (U.K.)

The main contributors from CASA were Enrique Rey, Fernando Monjas and Felix Lamela and, from DETyCOM, C. Martin Pascual and C. Cagigal. We also received very active support from C. G. M. van't Klooster from the Electromagnetic Division of ESTEC Technical Directorate.

We are grateful to James Lequeux, Philippe Zarka, Alain Lecacheux, and B. Rickett for their scientific and technical insights.

1

INTRODUCTION

Observing in a new electromagnetic waveband has always opened up new vistas in astronomy. The first radio astronomy observations were performed by Karl Jansky in 1932. He observed in the 20 meter band (15 MHz). Since that time radio astronomy has grown to a major scientific discipline and the frequency range has risen upwards with time. The observable band has moved only little to the lower frequencies because of the opacity of the ionosphere. Typically the cut-off is rarely goes below 10 MHz during the day and a few MHz during the night except at some exceptionally good observing locations. Many of the low frequency bands though once accessible are now drowned by man made transmissions and interference.

Radio astronomy has essentially moved to higher frequencies, not because of the lack of interest of the low frequency band but simply because spatial resolution has been much easier to reach at higher frequencies, since the angular resolution of an instrument is directly proportional to the wavelength.

Until now radio observations from space have been more modest in scope than those enjoyed in the optical region of the spectrum. This is mainly due to the longer wavelength of the radiation. To obtain a good sensitivity and directivity the collecting antenna must be large or else a series of antennas must be connected interferometrically together. Up to now this has been difficult to implement.

The possibility of using the far side of the moon as a base for radio astronomy certainly dates back to the recognition that man-made interferences could severely disturb radio astronomy observations. This is true for the entire radio astronomy window extending from millimetre wavelengths to decametre wavelengths. A lunar far side radio astronomy observatory is surely the dream of any radio astronomer on earth.

The low frequency band, however, permits the study of phenomena not manifested in any other spectral band, including low energy cosmic ray particles, thermal environment of discrete radio sources and coherent radiation arising from collective plasma processes, for a wide variety of both galactic and extra-galactic sources. Large scale distributions of thermal and relativistic gas in the interstellar medium can be traced from the study of absorption and scintillation near the low frequency end. This window is also particularly well suited for solar and planetary studies, including the earth's magnetosphere, and it brings a new method of detecting planets in other stellar systems. In what follows, we summarise some of the most important questions to be addressed.

2

SCIENCE PROGRAM

As demonstrated in the past by space missions exploring a new window (e.g. Einstein for X-rays, IRAS for infrared), not all science can be predicted and quantified. With this first high resolution view of the universe at very low frequency, one should, therefore, expect the unexpected.

With this in mind, it is still possible to define areas of research where observations at very low frequencies would make extraordinary contributions. This has been the subject of number of previous reports and conferences (e.g. in particular Burns, 1989; Kassim and Weiler, 1990; Erickson and Cane, 1989; Barrow et al., 1994). We review the highlights of these analyses in what follows.

2.1. Introduction to VLF radio astronomy

Very low frequency (VLF) radio astronomy is defined here as the frequency range below about 30 MHz, or the wavelength range above 10 m. We note that this definition, which is being used by radio astronomers, is rather loose and is totally different from the VLF range used by the radio electricians. Table 2.1shows a few typical frequencies and the corresponding wavelength regimes:

Table 2.1 The frequency/wavelength regimes

Frequency	Wavelength band	Denomination
30 MHz	10 m	decametric
3 MHz	100 m	hectometric
300 kHz	1 km	kilometric
30 kHz	10 km	

This is the last window of the electromagnetic spectrum never to have been observed with spatial resolution. Indeed, in this frequency range, radio astronomy from Earth-based observatories ranges from impossible at frequencies less than 2 MHz (because of ionospheric absorption and reflection), to extremely d-ifficult at frequencies of less than 100 MHz (because of man-made interference) - Figure 2.1.

Observations in this range have been attempted from the ground, down to a few MHz, sometimes with some success, but most of the knowledge that we have about the radio sources particularly below 1 MHz, comes from radio astronomy receivers on spacecraft in orbits well above the terrestrial ionosphere.

The antenna on spacecraft are usually wire antennas from a few meters long to a few hundreds of meters long. Hence, the sensitivity of such instruments is low and, above all, the instruments have no resolution (dipole antenna). A basic problem, at long wavelengths, is the absence of resolution, obtained only through interferometry : the resolution a of an instrument is

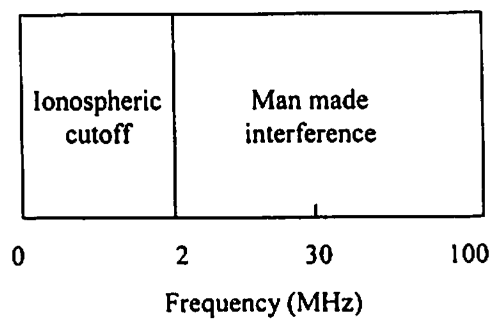

Fig. 2.1 Ionospheric absorption and man-made interference prevent very low frequency observations from the ground.

given, approximately, by $a = \lambda/D$, where λ is the wavelength, D is aperture, or baseline. As a rule of thumb, a resolution of 1 degree is obtained with an instrument whose aperture is roughly equal to 60 times the wavelength.

Intense, sporadic sources are easily identified. They originate from solar disturbances that propagate through the interplanetary medium, and from radiation near magnetised planets, including the Earth (Bougeret, 1990, 1993, 1996 ; Lecacheux, 1994). All other sources, galactic or extra-galactic, merge into a background which is well observed but not resolved to better than about 60 degree (the angular resolution of a dipole antenna whose length is short as compared to the wavelength). This background, called the "Galactic Background" (Brown, 1973) represents the actual limit to the sensitivity of receivers, which is thus not of instrumental origin. Figure 2.2, compiled from several references (Bougeret, 1993; Zarka, 1992. Lecacheux, 1994; Bougeret, Fainberg and Stone, 1984; Burns, 1990) shows the overall typical spectrum of the flux density of a variety of sources which are commonly observed. The background noise level is determined by the galactic background above 100 kHz and by the thermal noise of the local electrons on the antenna below 100 kHz. The Figure also shows the Auroral Kilometric Radiation (AKR), typical spectra of the magnetised planets, and an example of a type III solar radio burst. Radio phenomena at long wavelength consist essentially of the Galaxy, galactic and extra-galactic sources, planets, the Earth's magnetosphere, solar bursts in the interplanetary medium, local noise from the thermal electrons in the plasma surrounding the antenna. Several examples are given of astrophysical objects which show a steep spectrum down to the ionospheric cut-off. It is quite clear that the shape of their spectra (e.g. turnover frequency) contains much astrophysical information, some of which will be discussed below.

As already mentioned, measuring the direction and structure of the source is very difficult at low frequencies. Direction finding techniques are now currently used on spinning spacecraft. From the analysis of the modulation of the radio signal over a spacecraft spin, it is possible to deduce the source direction, an estimate of the source angular size, and its degree of circular polarisation (Manning and Fainberg, 1980). There have also been few successful attempts at interferometry (Baumback et al., 1986).

Figure 2.3gives the angular resolution of several existing radio interferometer arrays as a function of frequency. The resolution vs frequency dependence is shown for a variety of baselines. Cut-off frequencies are shown, including the ionospheric cut-off (about 10 MHz), the solar wind cut-off at 1 AU (1 Astronomical Unit), which is about 30 kHz, and the cut-off at the Heliopause

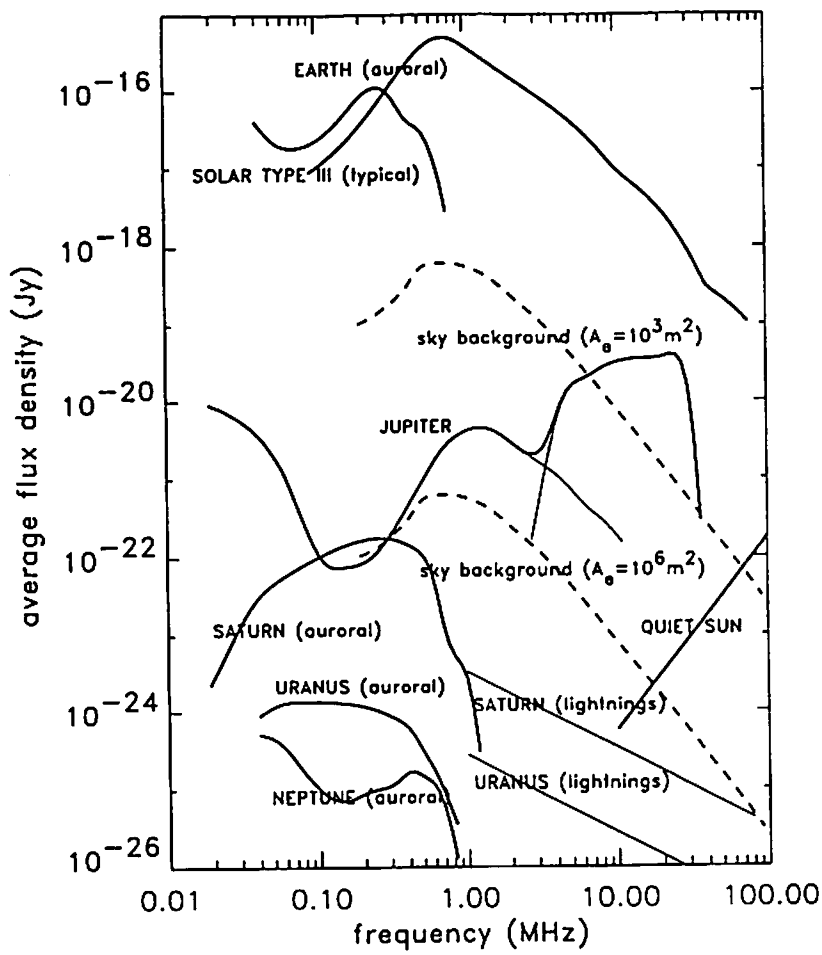

Fig. 2.2 Flux densities of typical radio sources in the range from 10 kHz to 100 MHz.

(about 3 kHz), corresponding to the lowest frequency that can penetrate into the Heliosphere. The electromagnetic radiation is strongly affected by both interstellar (ISS) and interplanetary (IPS) scattering, as will be discussed later. The magnitudes are shown on the figure by the lines ISS and IPS, whose slopes are about -2 in the log-log scale. The source-blurring is dominated by interplanetary scattering. For instance, it causes a point source at 1 MHz to have an apparent size of about 0.5 degree. This, in turn, sets an upper limit to the useful length of an array as a function of frequency.

Radio astronomy in general gives access to the disturbed universe; it involves non-coherent processes (and possibly coherent processes as will be discussed later) related to violent phenomena involving energetic particles.

The VLF band contains a lot of information which is not manifested in any other wavelength regimes, principally related to the fact that this band contains the turnover spectra of many sources, either intrinsic to the radiation

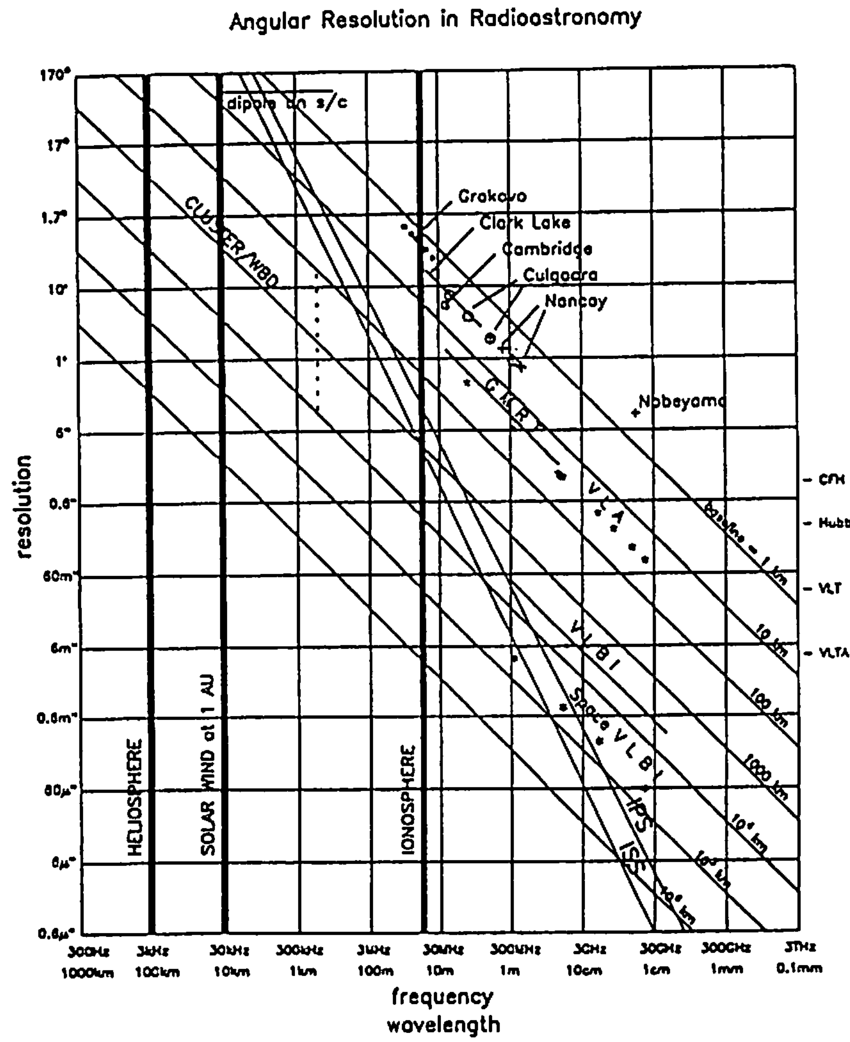

Fig. 2.3 Angular resolution of several radio interferometer arrays as a function of frequency.

mechanism, or because of absorption effects along the line of sight. VLF observations are most sensitive to the relativistic electron component of the cosmic rays and the distribution of the interstellar medium (Weiler et al., 1988).

Very little is known about the properties of individual radio sources at low frequencies. Thousands of sources are to be expected in the low frequency range. This is especially important, since the relativistic electrons that will be detected from their radio emission are, in general, far older than those normally studied by radio astronomy. Thus "fossil", steep spectrum sources which are not observable at higher frequencies, may become available for study with an impact on theories for the evolution and lifetimes of radio sources and of the universe (Dennison et al., 1986)

In what follows, we discuss some basic questions and problems that demonstrate the importance and uniqueness of this yet unexplored range to answer some basic questions about the Universe, our Galaxy, cosmic rays, etc.

2.2. The Universe at low radio frequencies

2.2.1 Plasma effects

A number of plasma effects are particularly efficient in the VLF range. They can modify the source spectra. Such effects can be intrinsic to the source and due to the source environment and to propagation effects. They are summarised below, as discussed by Duric (1990).

Free-free absorption

Plasma between the source and the observer can absorb radiation through free-free transitions. The optical depth of such a plasma is given by

$$\tau = 6.5 \times 10^5 T_e^{-1.35} \nu^{-2.1} \int n_e^2 dl \tag{2.1}$$

(using SI units), which is unity at a frequency

$$\nu = 5.21 \times 10^{-7} T_e^{-0.64} \left(\int n_e^2 dl \right)^{0.48} \mathrm{GHz} \tag{2.2}$$

where l is the path length in parsec and the other symbols have their customary significance (n_e is here in m^{-3}).

For the Galaxy, we may assume $T_e = 10^4$K and $n_e \sim 0.1\mathrm{cm}^{-3}$, giving a turnover frequency of 1 MHz in lines of sight through the galactic plane and about 200 kHz perpendicular to the plane. Thus, at 1 MHz, extra-galactic sources will be strongly attenuated when viewed through the plane. For standard HII regions, with higher electron densities, even the galactic background emission will be attenuated at frequencies an order of magnitude greater than this.

Suppression of radiation by a cold plasma

According to Tsytovitch (1951) and Razin (1960), relativistic electrons embedded in a plasma will suffer suppression of their synchrotron radiation below a critical frequency given by

$$\nu_c \simeq 20 n_e / B \mathrm{Hz} \tag{2.3}$$

For typical interstellar gas densities of $0.1\mathrm{cm}^{-3}$ and a transverse magnetic field $B \simeq 10^{-6}\mathrm{G}, \nu \simeq 10^5\mathrm{Hz}$. However, if the environments where particles radiate have higher electron densities or lower magnetic fields, this effect could be expected at higher frequencies. The effect could be searched for in galactic supernova remnants and in active galactic nuclei and would be recognised by the unique spectral shape. Measurement of ν_c and, for instance, an equi-partition calculation of B could yield the thermal gas density.

Synchrotron self-absorption

The importance of synchrotron self-absorption at low frequencies is that it is likely to affect virtually all extra-galactic sources and not just those extremely compact sources that commonly show the effect at very high (GHz) frequencies. A source is opaque to its own synchrotron radiation at a frequency

$$\nu_s \propto S^{2/5} B^{1/5} \theta^{-4/5} \mathrm{MHz} \tag{2.4}$$

At the higher frequencies, the self-absorbed spectrum rarely reaches the theoretical shape $S \propto \theta^{2.5}$ because different components reach self-absorption at different frequencies. This dilution will be less at VLF, but must nevertheless be accounted for. Once the self-absorbed components have been identified, it may be necessary to measure their angular sizes at higher frequencies. When this is done the magnetic field may be derived.

Coherent emission

As discussed by Dennison et al. (1986), a very exciting possibility at low frequencies is the detection of coherent radiation processes. There are valid physical reasons to anticipate that the smaller distance between individual radiating electrons, measured in terms of the electromagnetic wavelength is likely to amplify collective radiative modes. In such a plasma, the ratio of stimulated emission to spontaneous emission can be very high, varying as ν^{-3}. If an inverted energy level population can be established and is sufficiently long lived, there are numerous collective modes which can be excited by instabilities in the magneto-active plasma. Enhanced radiation should be generated at critical frequencies such as the plasma and gyro resonances and, in an inhomogeneous medium or in the non- linear case, coupling between modes can occur to produce wave amplification. In fact, the occurrence of coherent emission at low frequencies appears to be the rule rather than the exception for solar system objects such as the Sun, the major planets, and the magnetosphere of the Earth. Since objects such as the Crab Nebula, Seyfert galaxies, and quasars typically have densities of about 10^4 to $10^5 cm^{-3}$ and magnetic fields < 1 Gauss, we may anticipate an analogous situation leading to coherent plasma phenomena in the 1 to 3 MHz range.

2.2.2 The Galaxy and galactic sources

Galactic Non-thermal Background

Our Galaxy is pervaded by high-energy particles, the cosmic rays, and radio observations of the galactic background are directly related to the electron component of this relativistic gas and to the distribution of interstellar magnetic fields. This has been shown by several studies at frequencies down to about 30 MHz (Milogradov-Turin and Smith, 1973 ; Jones and Finlay, 1974) and has been reviewed by Dennison et al. (1985).

It has been shown, for example, that there is a good correlation between the energy spectrum of the cosmic ray electrons detected in the solar vicinity and the flux density spectrum of the non-thermal galactic radio background. Even here, however, there are problems in explaining the observed break in the cosmic ray electron energy spectrum near 3 GeV since neither attributing it to existing loss mechanisms nor ascribing it to the initial injection spectrum is completely satisfactory (see, e.g., Longair, 1981). Since this energy break is equivalent to the observed break in the background radio spectrum, low frequency observations may be able to distinguish regions in the Galaxy with different spectral properties and provide clues to the relevant loss and injection mechanisms. Existing surveys do not have sufficient resolution or provide sufficient spectral range to do this.

Hence, high resolution surveys in the low frequency range will not only allow us to define spectral indices with high precision, but will also give information on the distribution of different components of the galactic background.

For example, by measuring spectral index values and distributions, it should be possible to test theories as to whether the loop- like features seen in the background are old remnants from nearby supernovae (Berkhuijsen, 1971) or loops of magnetic field and particles leaking out of the galactic plane (Parker, 1965). Also, at low frequencies the non-thermal halo of the Milky Way will be prominent and it should be possible to measure its extent, relativistic particle density and magnetic field strength for a better determination of the confinement mechanisms for cosmic ray electrons and protons. It must be remembered that, at the low frequencies which we propose to observe, the lifetime of the synchrotron electrons is a significant fraction of the age of the universe, so that we will be studying distributions relatively unaltered by evolutionary effects.

Galactic Diffuse Free-Free Absorption

It has been suggested by Acanison et al (1985) that, by observing a large number of extra-galactic radio sources and determining their low frequency spectra as a function of galactic latitude and longitude, it should be possible to measure the changes due to absorption by the diffuse, interstellar gas in the Milky Way and hence investigate its distribution. While, near 1 MHz, this interstellar absorption may affect survey results of the non-thermal background in the galactic plane, we expect that, by combining the survey results at the several frequencies, including higher frequency maps from the literature, we can successfully separate the thermal absorption and non-thermal emission components of the Galaxy. Thus, models for a "warm" ($T_e \simeq 10^4$K) disk of ionised hydrogen imbedded in a "hot" ($T_c \simeq 10^6$K) halo can be tested and a global picture of the free-free absorption obtained for comparison with existing higher frequency pulsar dispersion and Faraday polarisation rotation measurements. These results will be supplementary to the COS-B γ-ray measurements which are related to the local cosmic ray energy and interstellar gas density.

A complementary technique to the study of the diffuse free-free absorption would be to use nearby HII regions, which are optically thick at these low frequencies, completely to block the non-thermal background radiation from more distant parts of the Galaxy. Then, any emissivity observed can be attributed solely to the synchrotron radiation arising between the observer and the HII region, yielding a measurement of local values of the cosmic ray electrons and magnetic field components.

Supernova Remnants: spectrum of low energy cosmic rays

Low-frequency observations of supernova remnants (SNRs) are of interest for studies of their intrinsic spectra, extending down in frequency thus giving information about the emission mechanism. A peculiarity at low frequencies, cited by Chevalier (1990), is the 38 MHz 'flare' observed in Cas A in the mid-1970's. Perhaps such events carry important clues for the understanding of radio emissions. Much more information is needed about phenomena such as this.

Absorption measurements are also important because of their bearing on the properties of the immediate neighbourhood of the remnants and the possible interaction of the SNR with its surroundings.

Duric (1990) discussed the effect of optically thin synchrotron radio emission, as follows. A high energy electron emits radiation via the synchrotron mechanism as a frequency given by

$$\nu = 10^{18} B E^2 \mathrm{Hz} \tag{2.5}$$

where B is the magnetic field strength, E is the electron energy and ν is the frequency at which the radiation spectrum of the electron peaks. The electron radiates away half its energy in a time given by

$$t_{1/2} = 8 \times 10^9 (\frac{B}{\mu G})^{-2} (\frac{E}{GeV})^{-1} \text{years.} \tag{2.6}$$

Combining these two equations gives

$$\nu_b = 3.4 \times 10^{26} (\frac{B}{\mu G})^{-2} (\frac{t}{years})^{-2} \text{Hz} \tag{2.7}$$

where ν_b represents the break frequency in a synchrotron spectrum resulting from the ageing of the electrons. For ν = 1 MHz and b = 1μG, a 0.5 GeV electron can exist for over 10^{10} years before losing most of its energy (inverse Compton losses off stellar and background photons reduce the lifetime, at the most, by a factor of 2 or 3). In principle, it is possible to study fossil electrons that have been around since the formation of the galaxies that gave rise to them. As discussed below, it may be possible to detect such electrons in galactic halos and in the lobes of radio galaxies.

Studies of VLF emission from supernova remnants (SNR) may prove useful in revealing the mid-energy component of the CR electrons that is not detectable from the Earth. For electrons radiating in 100 μG magnetic fields inside SNRs at 1 MHz, the expected energies are about 50 MeV. This is well below the solar modulation cut-off that eliminates studies of galactic cosmic rays below 1 GeV. The shape of the energy spectrum below 1 GeV is a critical constraint on CR acceleration theories and provides a bridge between the higher energy cosmic rays and the thermal electrons from which they have, presumably, been accelerated.

2.2.3 A strawman science plan for Very Low Frequency Radio Astronomy

In the previous sections, we have discussed a number of scientific questions and problems that could be answered by VLF observations. This list is certainly not exhaustive. It may still appear as a mere catalogue and priorities will have to be set to optimise the science return and to have as broad an impact on the scientific community as possible.

Even this may be a difficult exercise; the example of the X-ray precursor missions has shown that not all science can be predicted and quantified in advance. Serendipity is also a factor with the simple fact of opening a new window in the electromagnetic spectrum. A basic question is certainly, "what is the sky like *at all*, in this uncharted end of the spectrum?"

A simple plan could be as follows:

- Deep survey (IRAS type)
- nature of the radio sources with extreme spectral behaviour
- study of very old radio sources; measurement of old spectral ages from break frequency; discovery of high redshift clusters

At a later stage, when a more complete instrument is available:

- high resolution survey
- search for unusual objects and active phenomena.

2.3. Solar system

2.3.1 Low frequency radio sources within the solar system

The Voyager Planetary Radio Astronomy (PRA) experiment has demonstrated that all four of the giant planets emitted radio waves within a band of frequencies extending from 1.2 to 1300 kHz in addition to the jovian decametre-wave radiation (DAM), already well-known from ground-based observations at frequencies of a few MHz up to 40 MHz. The characteristic spectra of the radio emissions from the giant planets are shown in Figure 2.2. Radio emission from the Earth has also been detected by several spacecraft, for example the Imp 6 and 8 satellites and, more recently, by Viking. Flux densities normalised to 1 A.U. are, typically, about 10^{-18} to 10^{-20} W m^{-2} Hz^{-1} for Jupiter, 10^{-21} W m^{-2} Hz^{-1} for Saturn and the Earth, and an order of magnitude lower for Uranus and Neptune. Solar radio emission can be even more intense than jovian emission with type III burst flux densities of the order of 10^{-17} W m^{-2} Hz^{-1} or even higher at kilometric frequencies. Frequency ranges and flux densities are given in detail in the first report of the ESA Science Team on the project "Very low frequency lunar observatory" (Barrow et al., 1994a).

Both solar and planetary radio emissions contain a number of different components, each of which displays distinctive spectral characteristics. A number of Earth-based observations of the Sun (at metre- and decametre-wave frequencies) and of Jupiter (at decametre-wave frequencies) have shown the presence of complex fine structures in the radiation. See, for example, for the Sun, Ellis (1969), McLean (1985), Barrow et al. (1994b) and, for Jupiter, Riihimaa (1992). Apart from the jovian DAM, all radio emission from the giant planets is confined to kilometric frequencies and cannot, therefore, be received at the Earth as it is always below the critical frequency of the ionosphere. Although a certain amount of general investigation has been possible from spacecraft such as Voyager and Ulysses, high time and frequency resolution observations have not so far been attempted from space. The Sun, of course, has been studied extensively from the Earth (Krüger, 1979) at all wavelengths above the critical frequency and at longer wavelengths from space but, again, with very limited time resolution. There is no reason to suppose that fine structures should not exist down to lower frequencies and the VLFA system should have the necessary resolution for investigating these in detail as far as possible.

The effects of interplanetary scattering will set a limit to what can be resolved at lower frequencies, however. According to Section 4.1.2, the temporal broadening in seconds is $\tau_b = 0.1f^{-4.4}$ where f is in MHz; whence the lowest frequency at which a 5 ms structure could be resolved would be about 2 MHz. For 250 kHz, the corresponding time resolution would be about 45 s. Below about 250 kHz, the small angle approximation (see Section 4.1.2) would no longer be valid and the values of τ_b would be lower than those predicted by the equation. At 100 kHz it is estimated that τ_b would be reduced by a factor of about three, that is from about 42 min to 14 min, but also depending upon interplanetary medium conditions at the time. These figures are discouraging but, on the other hand, nothing is known about temporal fine structures much below 15 MHz and these could be readily detected down to about 2 MH. Also, a structure does not have to be fully resolved to be detected, of course. Voyager revealed that there are numerous components of planetary radiation at kilometric frequencies which can be studied with considerably longer time resolution. The jovian DAM certainly extends down to 5 MHz and may continue to lower frequencies, possibly merging into the jovian hectometric emission

(HOM). Also, it must be remembered that there have been very few observations of solar radio emission at any frequencies between about 20 MHz, the low-frequency limit of most observations from the Earth, and 2 MHz where, prior to the WIND mission, most spacecraft observations commenced.

The investigation of polarisation is essential as this can provide insight to magnetic conditions at the Sun and within a planet's magnetosphere. Below about 1 MHz, scattering effects will influence the measurement of the polarisation angle through broadening of the Faraday rotation angle although the actual sense of the polarisation observed should not be affected (See Sections 4.1.3, 4.1.4). Measurements at the lower decametric frequencies (15 to 2 MHz) would represent a considerable advance on measurements made from the Earth, however, and all of the Stokes' parameters should be measurable in this frequency range providing that the receiver bandwidth is not so large that Faraday rotation within the bandwidth became serious (Cohen, 1958).

There are certain aspects of planetary radiation, such as possible secular variation in the rotation period, which may need long-term observation (see, for example, Carr and Wang, 1990; Barrow and Carr, 1992; Barrow and Lecacheux, 1995). Also, observations of Uranus (Desch et al., 1992) and Neptune (Lecacheux and Pedersen, 1992) have been confined to relatively short periods close to encounter by Voyager 2. Lecacheux (1994) has reviewed some of the possibilities for lunar-based observations. Certainly, there is much interesting work awaiting detailed investigation in the study of low frequency solar system sources.

2.3.2 Scientific Programme

The research possibilities within the different frequency bands are as follows:

30 to 15 MHz: Solar and jovian radio emission

(a) Comparison of lunar-based observations with Earth-based observations of the Sun and Jupiter

15 to 1 MHz: Above the most serious scattering effects and the least studied frequency band to date

(a) Good frequency and time resolution possible ($\tau = 5$ ms at 2 MHz, 0.1 s at 1 MHz) and all four Stokes' polarisation parameters measurable

(b) Solar emission: Spectra, low frequency extent of different burst types, fine structures and polarisation of the different burst-types

(c) Planetary emission: Predominantly Jupiter in this frequency band

1. Long term monitoring of jovian HOM close to 1 MHz to search for a possible secular variation in the rotation period
2. Changes in jovian CML occurrence probability profiles below 15 MHz
3. Spectra, fine structures and polarisation of the jovian emission
4. Emission from Saturn and Neptune is weak and uncertain above 1 MHz
5. No emission has been detected from Uranus above 1 MHz.

1 MHz to 100 kHz:

(a) Solar emission: Spectra and low frequency extent of different burst-types; fine structures and polarisation as far as possible, bearing in mind IPS effects

(b) Planetary emission: All of the outer planets

1. Long-term monitoring for CML profiles of jovian and saturnian emission and possibly uranian and neptunian emission

2. Long term monitoring of the SKR and the jovian HOM close to 400 kHz to search for possible secular variations in the rotation periods
3. polarisation sense and other parameters as far as possible (IPS)
4. Characteristics of the numerous components of Uranus' radio emission in the frequency range 20 to 900 kHz
5. Characteristics of the two components of Neptune's radio emission in the frequency ranges 20 to 600 kHz (s-NKR) and 420 to 1300 kHz (b-NKR)

In addition, an interesting possibility exists in the observation of unresolved temporal fine-structures in planetary emission at lower frequencies, below about 250 kHz, say. This might be used as a check on scattering theory, by assuming that all the temporal characteristics observed (of the type shown by the bKOM) were due to scattering effects, for the known distance of the planet and the measured density of the solar wind. To date, measured values have not been available to verify the theory.

Ideally, the receiver used for solar system observations should cover frequencies belo v 100 kHz (see Figure 1) and so be comparable with the receivers on Ulysses and on WIND. A preliminary check, using Ulysses URAP and WIND/WAVES observations of the jovian bKOM emission when the spacecraft were several AUs from the planet, might allow the feasibility of this to be assessed.

References:

Alexander, J. K., and M. D. Desch, Voyager observations of Jovian millisecond radio bursts, J. Geophys. Res., 89, 2689, 1984

Barrow, C. H., and D. P. Morrow, The polarisation of the Jupiter radiation at 18 MHz, Astrophys. J., 152, 593, 1968

Barrow, C. H., and M. D. Desch, Solar wind control of Jupiter's hectometric radio emission, Astron. Astrophys., 213, 495, 1989

Barrow, C. H., and T. D. Carr, Radio observations of the Jovian magnetic field, Adv. Space Res., 12, (8)155, 1992

Barrow, C. H., J-L. Bougeret, Y. Leblanc, J-P. Lebreton, R. Laurance, M. Fridlund, S. Volonte, Very low frequency lunar observatory, Annex 1 to ESA Report PF/rjl/968, 1994a

Barrow, C. H., P. Zarka, M. G. Aubier, Fine structures in solar radio emission at decametric wavelengths, Astron. Astrophys., 286, 597, 1994b

Barrow, C. H., and A. Lecacheux, Problems concerning the radio emission from Jupiter observed by Ulysses after encounter, Astron. Astrophys., 301, 903, 1995

Baumback, M.M., D.A. Gurnett, W. Calvert, and S.D. Shawhan, 1986, Geophys. Res. Lett. 13, 1105.

Boischot, A., Y. Leblanc, A. Lecacheux, B. M. Pedersen, M. L. Kaiser, Arc structure in Saturn's radio dynamic spectra, Nature, 292, 727, 1981

Bougeret, J.-L., 1993, Adv. Space Res., 13, (6)191.

Bougeret, J.-L., 1990, in Astrophysics from the Moon, eds. M.J. Mumma and H.J. Smith, AIP Conference Proceedings, 207, 139.

Bougeret, J.-L., 1996, Adv. Space. Res., 18, (11)35.

Bougeret, J.-L., Fainberg, J., and Stone, R.G., 1984, Astron. Astropys., 136, 255.

Brown, L.W., 1973, ApJ, 180, 359.

Burns, J.O., 1990, in Astrophysics from the Moon, eds. M.J. Mumma and H.J. Smith, AIP Conference Proceedings, 207, 207.

Burns, J.O., *A lunar far side very low frequency array*, NASA Pub 3039, Proc. workshop Albuquerque, J. Burns Ed. 1989.

Carr, T. D., and L. Wang, in *Low Frequency Astrophysics from Space*, edited by N. E. Kassim and K. W. Weiler, p. 113, Springer, Berlin, Heidelberg, New York, 1990

Cohen, M. H., Radio astronomy polarisation measurements, Proc. I. R. E., 46, 172, 1958

Dennison, B.K., K.W. Weiler, K.J. Johnston, R.S. Simon,J.H. Spencer, L.M. Hammarstrom, P.G. Wilhelm, W.C. Erickson, M.L. Kaiser, M.D. Desch, J. Fainberg, L.W. Brown, and R.G. Stone, 1986, NRL Memorandum Report 5905.

Desch, M. D., M. L. Kaiser, P. Zarka, A. Lecacheux, M. Aubier, and A. Ortega-Molina, Uranus as a radio source, in *Uranus*, edited by J. T. Bergstralh, E. D. Miner, and M. S. Matthews, p. 894, Univ. of Arizona Press, 1992

Duric, N., and J.O. Burns, Very low frequency radio astronomy from lunar orbit, Engineering, Construction and Operations in Space, IV, Proceedings of Space, 94, vol 2, edited by G. Galloway and S. Lokaj, 19??.

Duric, N., 1990, in Astrophysics from the Moon, eds. M.J. Mumma and H.J. Smith, AIP Conference Proceedings, 207, 515.

Ellis, G. R. A., Fine structures in the spectra of solar radio bursts, Aust. J. Phys., 22, 177, 1969

Erickson and Cane, *Low frequency radio astronomy*, Proc. Workshop, NRAO Green Bank, 1984.

Fainberg, J., and R. G. Stone, Satellite observations of type III solar radio bursts at low frequencies, Sp. Sc. Rev., 16, 145, 1974

Jones, B.B., and Finlay, E.A., 1974, Aust. J. Phys., 27, 687.

Kaiser, M. L., The Radio Astronomy Explorer program: valuable lessons for future low frequency radio astronomy from space, in *A lunar far-side very low frequency array*, edited by J. O. Burns and N. Duric, p. 23 NASA Conference Publication 3039, 1989

N. E. Kassim and K. W. Weiler, *Low Frequency Astrophysics from Space*, Springer, Berlin, Heidelberg, New York, 1990

Krüger, A., *Introduction to solar radio astronomy and radio physics*, Reidel, Dordrecht, 1979

Lecacheux, A., and B. M. Pedersen, Neptune as a radio source, in *Planetary Radio Emissions III*, edited by H. O. Rucker, S. J. Bauer, and M. L. Kaiser, p. 281, Austrian Academy of Sciences Press, Vienna, 1992

Lecacheux, A., Solar system low frequency radio astronomy from the moon, Adv. Space Res., 14, (6)193, 1994

Lecacheux, A., 1994, Adv. Space Res., 14, (6)193.

Manning, R., and Fainberg, J., 1980, Space Sci. Inst. 5, 161.

May, J., T. D. Carr, and M. D. Desch, Decametric radio measurements of Jupiter's rotation period, Icarus, 40, 87, 1979

McLean, D. J., Metrewave solar radio bursts, in *Solar Radiophysics*, edited by D. J. McLean and N. R. Labrum, p. 37, Cambridge University Press, Cambridge, 1985

Milogradov-Turin, J., and Smith, F.G., 1973, MNRAS, 161, 269.

Nelson, G. J., and D. B. Melrose, Type II bursts, in *Solar Radiophysics*, edited by D. J. McLean and N. R. Labrum, p. 113, Cambridge University Press, Cambridge, 1985

Nelson, G. J., K. V. Sheridan, and S. Suzuki, Measurements of solar flux density and polarisation, in *Solar Radiophysics*, edited by D. J. McLean and N. R. Labrum, p. 113, Cambridge University Press, Cambridge, 1985

Piddington, J. H., *Radio Astronomy*, Harpers, New York, 1961

Riihimaa, J. J., Wide-range high-resolution S-burst spectra of Jupiter, Department of Astronomy Report, University of Oulu, 1992

Stone, R. G., et al. (31 co-authors), Astron. Astrophys., 92, 291, 1992

Weiler, K.W., B.K. Dennison, K.J. Johnston, R.S. Simon, W.C. Erickson, M.L. Kaiser, H.V. Cane, M.D. Desch, and L.M. Hammarstrom, A low frequency radio array for space, Astron. Astrophys., 195, 372-379, 1988.

Zarka, P., The auroral radio emissions from planetary magnetospheres: What do we know, what don't we know, what do we learn from them?, Adv. Space Res., 12, (8)99-(8)115, 1992

3
WHY THE LUNAR FAR SIDE?

Since the start of man-made radio communications, the radio spectrum has become more and more polluted.

In particular, because long waves are blocked by the ionosphere up to a few Megahertz, they have been used as the most attractive media for broadcasting radio messages all around the world.

To overcome interference from other stations, the power, utilised by each of these transmitters, has been raised by orders of magnitude above the minimum level required to reach the receivers. This is still true nowadays for the less developed countries.

In fact, the most advanced applications require many new and wider transmitting channels that can be accommodated only on the microwave part of the radio spectrum via relay satellites, usually orbiting near the Earth in geosynchronous orbits.

Because radio astronomy collects the radio energy emitted by celestial objects, it is an essentially passive (only receiving) activity. Thus the two previous facts, ionospheric shielding and extremely high level of man-made interference, have always prohibited any radio astronomical research at the low frequency end of the radio spectrum.

To overcome this problem, it seems particularly attractive to locate a radio telescope on the far side of the Moon. There one can count on geometrical shadowing, by the Moon itself, from the noise generated on the Earth.

The region on the lunar surface where this will happen is limited by various factors: (1) the libration exposes a few degrees in longitude of the limb; (2) the so called "knife-edge diffraction", due to asperities in the limb region, extend the region where some radio flux can still be received (Hall, 1985); (3) scattering from small scale inhomogeneities of the magnetosphere can bend the propagation of radio waves of extremely low frequency (below 500 kHz) as, for example, in the AKR from the Earth. This last effect has only marginal importance in the VLFA design and operation, however.

Only the first two factors need be considered in the evaluation of how near to the limb it is possible to locate the VLFA.

It is extremely important from now on, to keep the far side of the moon free from all installation of radio transmitters which could radiate in the shielded zone of the Moon.

The protection must cover all frequencies inaccessible from the Earth, at both the lower and the upper end of the radio spectrum; in particular the former as far as the VLFA project is concerned.

Some intermediate band must be left available to the radio links needed for the exploration of the far side of the Moon itself. The nominal 15 GHz links, between the receiving elements of the VLFA and the central station, are an example.

With this in mind, we have contacted the scientific and technical advisory committees of the ITU (International Telecommunication Union), the IUCAF

(Inter-Union Commission on Frequency Allocations for Radio Astronomy and Space Science) – (Ponsouby, 1994) and the CRAF (European Science Foundation's Committee on Radio Astronomy Frequency) – (Ponsouby, 1995).

These organisations are now aware of the VLFA project and they guarantee that all needed actions will be taken to keep the radio spectrum clean in the frequency range to be investigated by the VLFA.

Locating VLFA at the L2 Lagrangian point, as a free-flyer mission, would not have any advantage from the point of view of radio shielding from man made or natural sources of radio noise, with respect to a location on the far side of the Moon.

In fact the ratio between the distances from L2 and the Earth and from L2 and the Moon, combined with the Moon and Earth radii, do not allow any significant geometrical shadowing. Also the additive free path loss does not give more than 14dB of attenuation to the Earth interference, as heard from L2.

The only possible alternative would be a cluster of antennas orbiting at low altitude around the Moon.

References

Hall M.P.M. "Effects of the troposphere on radio communication", P. Peregrinum LTD, pp 151-157, 1985

Ponsouby, J.E.B., "The shielded zone of the Moon", IUCAF document No 407, with appendix 2 and 3, 1994.

4

DESIGN CONSIDERATIONS

4.1. Scattering effects in turbulent plasmas

4.1.1 Angular broadening

Low-frequency radio astronomy demands a careful consideration of the effects on the observations of various turbulent plasmas, notably the ionosphere, the interplanetary medium and the interstellar medium. At frequencies well above their plasma frequencies, density fluctuations in the plasmas lead to variations in refractive index that scale as the wavelength squared, so the effects are most severe at the lowest frequencies.

In general, a region of space in which the electron density deviates by ΔN_e from the mean gives rise to a change in refractive index of

$$\Delta\eta = -\frac{r_e}{2\pi}\lambda^2\Delta N_e \tag{4.1}$$

where r_e is the classical radius of an electron (2.82×10^{-15} m) and λ the wavelength of the radiation. To see how this affects radio propagation it is useful to imagine all the density fluctuations from an extended region of space to be compressed to a 'thin screen' of thickness L at some distance z along the line of sight to the radio source (Figure 4.1). We may further simplify the model by assuming a scale-size of a for the density inhomogeneities (or blobs, from now on). This is the so-called 'Gaussian thin-screen model' and displays all the major functional relationships between the radio waves and the plasma.

We see that there is an excess change of phase, $\Delta\phi$, of $2\pi\Delta\eta a/\lambda = r_e\lambda a\Delta N_e$ through each blob relative to the free-space path, and each part of the wave-front incident on the thin screen encounters about L/a blobs. If the blobs are arranged randomly this introduces phase fluctuations of

$$\Delta\phi_{\rm rms} = \sqrt{\frac{L}{a}}r_e\lambda a\,\Delta N_e = r_e\lambda\,\Delta N_e\sqrt{La} \tag{4.2}$$

over the screen by the time the wave-front has emerged. At frequencies below 10 MHz we expect the magnitude of these phase fluctuations to be large in the interstellar and interplanetary medium ($\Delta\phi \gg 1$) so the effect is one of a random assembly of small prisms, each deflecting the radiation over a characteristic angle

$$\theta_s = \frac{\lambda\Delta\phi}{2\pi a}. \tag{4.3}$$

This 'strong scattering' therefore spreads the radiation from a point source over a solid angle of characteristic width

$$\theta_s = \frac{r_e}{2\pi}\lambda^2\Delta N_e\sqrt{\frac{L}{a}} \tag{4.4}$$

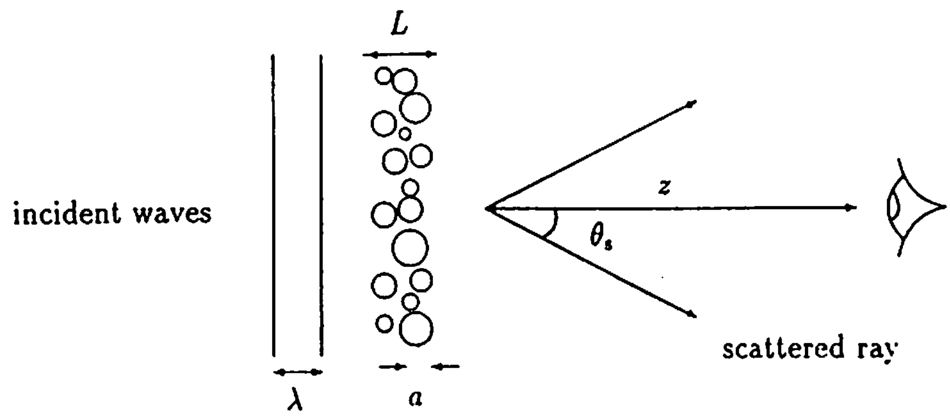

Fig. 4.1 Geometry of the Gaussian 'thin screen' model.

A possibly more realistic model uses a Kolmogorov power law for the spatial spectrum of the density fluctuations rather than a fixed scale-size, a. This results in a similar relation, but with $\theta_s \propto \lambda^{2.2}$ rather than λ^2. The result can be usefully expressed in terms of the integral of the 'turbulence strength' of the medium, C_N^2, along the line-of-sight to the source. This gives a scattering angle of (D is the distance to the source)

$$\theta_s \simeq 4.1 \times 10^{-13} \left(\int C_N^2(x)(x/D)^{5/3}\, dx \right)^{3/5} \lambda^{11/5} \text{ arcsec} \tag{4.5}$$

Once we are outside the Earth's ionosphere, the two most important plasma regions that affect radio propagation are the interplanetary medium (IPM) and the interstellar medium (ISM). Both have been observed extensively at decimetric wavelengths (e.g., Cordes 86, Erickson 64, Rickett 77), allowing us to calibrate the above expressions for θ_s.

Under the conditions of strong scattering that we expect at decametric and longer wavelengths (i.e., below 30 MHz) we have:

Mode	θ_s
interplanetary scattering	$\sim 100/(P\nu_{\mathrm{MHz}})^2$ arcmin
interstellar scattering	$\sim 22/\nu_{\mathrm{MHz}}^2$ arcmin

where P is the 'impact parameter' of the line of sight to the source relative to the Sun in AU (i.e., about 1). Again we use the Gaussian model, but the two models (Gaussian and Kolmogorov) give roughly similar results over the frequency range considered. We see from this that interplanetary scattering dominates over interstellar scattering by a factor of about 4 (Figure 4.2). Although interplanetary scattering changes with the solar elongation, most of the material that contributes to the scattering process is within about 1 AU of the Earth and can therefore be thought of as 'local'. The result is that interplanetary scattering does not vary greatly for elongations of more than about 90 degrees.

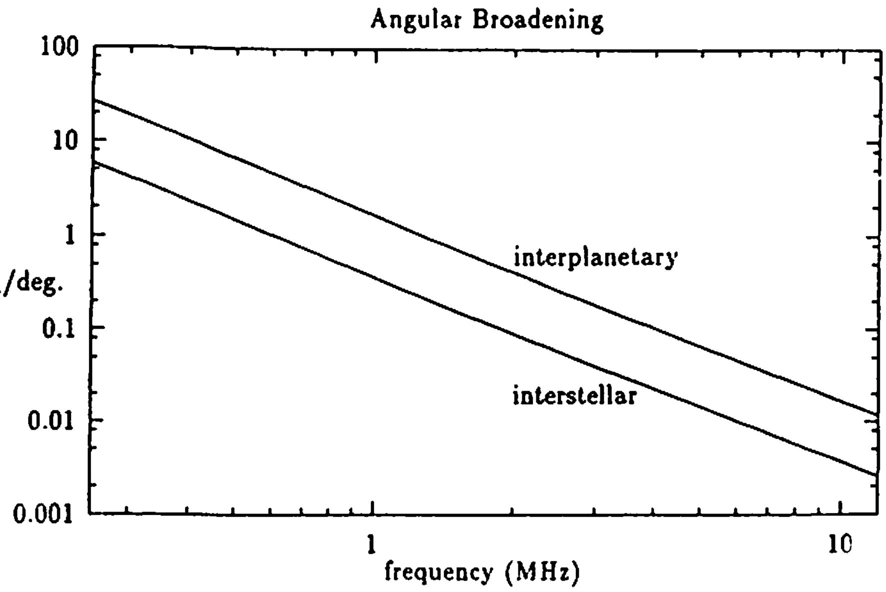

Fig. 4.2 Interplanetary and interstellar angular broadening (Gaussian model).

4.1.2 Temporal broadening

The scattered rays that broaden the angular size of a point source also give rise to *temporal broadening*. This arises from the range of propagation paths, and hence times, available between the source and the receiver, and will smear transient signals such as pulses from pulsars.

Small-angle approximations give the range in differential propagation times from a source at infinity, broadened to an angular extent of θ_s radians, as approximately

$$\Delta\tau_b = \frac{z\theta_s^2}{2c} \tag{4.6}$$

where z is the distance between the screen and the observer and c is the speed of light. For a screen at some distance z' from the source the expression is modified by using the *reduced distance*, $z^* = zz'/(z + z')$, in place of z.

Again, this expression can be given an approximate calibration using observations of pulsars and angular broadening at frequencies of a few tens of MegaHertz (Cordes 90), to give

Mode	$\Delta\tau_b$
interplanetary scattering	$0.1\,\nu_{\mathrm{MHz}}^{-4.4}$ seconds
interstellar scattering	$2\times10^{8}\nu_{\mathrm{MHz}}^{-4.4}$ seconds

using this time the Kolmogorov model ($\theta_s \propto \nu^{-2.2}$). The two relationships are shown graphically in Figure 4.3. We see that the vast distances involved in interstellar propagation make the effects of interstellar temporal broadening severe. At 1 MHz the temporal broadening is approximately equal to the proposed mission lifetime of 5 years. Clearly little, if any, temporal work can be done with extra-solar system objects at frequencies below 10 MHz. It is

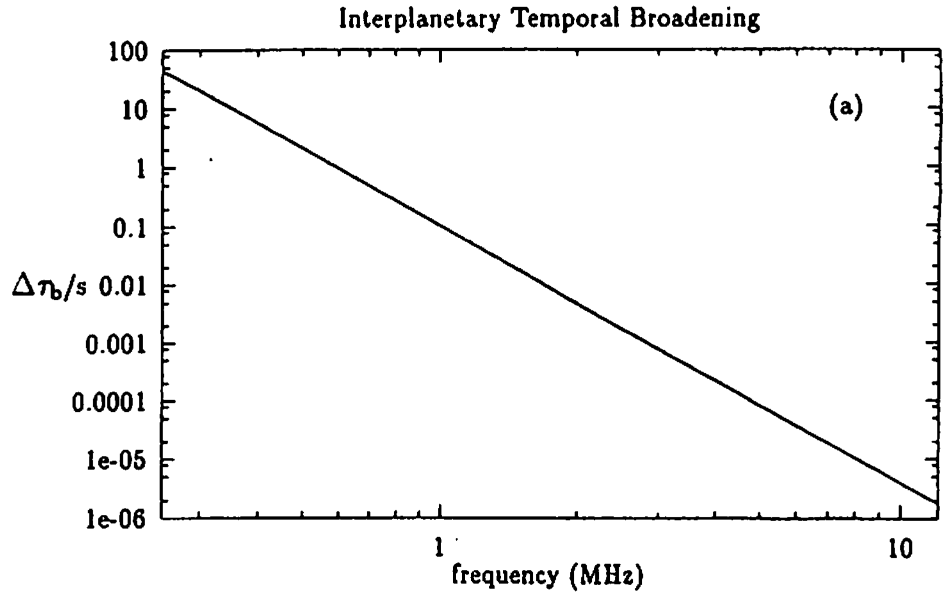

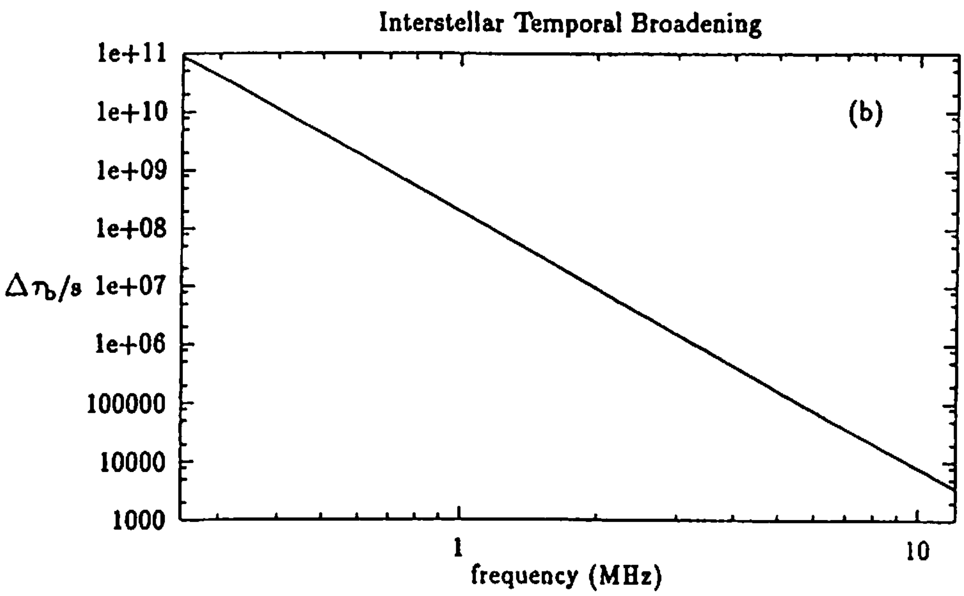

Fig. 4.3 Interplanetary (a) and interstellar (b) temporal broadening (according to the Kolmogorov model).

relevant to note that there are only three known pulsars that would *not* be smeared out in this way at 10 MHz.

Interplanetary temporal broadening is less severe, amounting to about 0.1 sec at 1 MHz and 10 seconds at 300 kHz. At still lower frequencies we cannot justify the small angle approximation involved in deriving Equation 4.6, but the effects of this are not too great—at 100 kHz the true temporal broadening is only about a factor of three less than that predicted by Equation 4.6.

4.1.3 Faraday rotation

The plane of polarisation of a wave propagating through a plasma will rotate due to 'Faraday rotation' if there is a magnetic field component, $B_{//}$, parallel to the direction of propagation. Explicitly,

$$\mathrm{FR} = \frac{2.36 \times 10^4}{\nu^2} \int N_e B_{//} \, dl \quad \text{radians,} \tag{4.7}$$

where ν is in Hz, N_e in m^{-3} and l in m. Within the solar system both N_e (from the solar wind) and B (also from the Sun) drop as $\sim 1/r^2$, so that the Faraday rotation is dominated by the near-Earth environment, giving

$$\mathrm{FR} \simeq \frac{46}{\nu^2_{\mathrm{MHz}}} \quad \text{radians,} \tag{4.8}$$

(this assumes $B \simeq 6 \times 10^{-9}$ Tesla and $N_e \simeq 6.5 \times 10^6 \,\mathrm{m}^{-3}$). In the antisolar direction, both N_e and B are highly variable quantities within the solar system, each changing by factors of 3 or 4 on time-scales of hours. This means that polarisation angle is poorly defined at these frequencies, although dual-frequency measurements may go some way to 'unwind' the rotation introduced at the higher frequency ranges.

On the other hand, circular polarisation remains well defined, the only effect of the intervening plasma being the introduction of a phase-lag between the two polarisation components. In the universe as a whole, circular polarisation is rarely seen. This is probably because the radiation mechanisms that generate it (mostly cyclotron processes) are not sufficiently energetic to produce bright sources. The more luminous synchrotron emission is therefore the dominant mechanism. Within the solar system, circularly polarised cyclotron emission from the Sun and planets can be detected, notably from Jupiter and Saturn, and this represents the clearest reason to include a polarisation measuring capability in the VLFA.

4.1.4 Faraday depolarisation

The radiation from a source can travel to the observer over a multiplicity of paths, each with its own, possibly different, Faraday rotation. This gives rise to (linear) Faraday depolarisation, which may be significant within the solar system at very low frequencies. Its effects within the solar system can again be approximated using the Gaussian thin screen-model for the interplanetary medium. From Equation 4.7, we see that each blob (scale-size a) in the screen (thickness L) will introduce a differential rotation of

$$\Delta\psi = \alpha \Delta N_e \lambda^2 a B_{//}, \tag{4.9}$$

where $\alpha = 2.6 \times 10^{-13}$ (assuming SI units). The analysis proceeds in a manner similar to that for angular broadening. The wave-front encounters about L/a blobs during its passage through the screen, giving the emerging wavefront a random polarisation structure with an rms polarisation angle of

$$\Delta\psi_{\mathrm{rms}} = \alpha \Delta N_e \lambda^2 a B_{//} \sqrt{\frac{L}{a}} \tag{4.10}$$

This can be combined with Equation 4.4 to give an expression in terms of scattering angle:

$$\Delta\psi_{\mathrm{rms}} = \frac{2\pi\alpha}{r_e} a B_{//} \theta_s \tag{4.11}$$

Taking a to be about 200 km for the IPM gives

$$\Delta\psi_{\rm rms} \simeq \frac{10^{-2}}{\nu_{\rm MHz}^2}. \tag{4.12}$$

Although not significant at frequencies greater than about 1 MHz this could be a limiting factor for linear polarisation measurements within the solar system at the lowest reaches of the VLFA frequency range. Furthermore it represents a fundamental limit to linear polarisation measurements as, unlike simple rotation, it cannot be removed by making dual-frequency observations. Circular polarisation is not affected by this process, so the circularly polarised emission from planets will be still be seen, although it will be diluted somewhat by unpolarised background emission.

On the larger scale, we do not expect to see any linear polarisation from galactic or extra-galactic signals. Both the amount of rotation and the degree of depolarisation scale as λ^2 at low frequencies (Tribble 91). If we take the galactic electron number density to be about 0.3×10^5 m^{-3} and the magnetic field about 5×10^{-10} T, a rotation of 1 radian would be seen over a plasma blob of size $\sim 10^{-3}$ pc at 3 MHz. As we can expect many such blobs within the telescope beam for all but the closest sources, the radiation can be expected to be linearly unpolarised. Furthermore, the total Faraday rotation over interstellar distances is large, amounting to about 10^4 radians per parsec at 1 MHz and scaling as λ^2. The *differential* rotation over the observing band is therefore correspondingly great. At 3 MHz, the differential rotation amounts to 1 radian over a 1 kHz bandwidth after only 0.4 pc.

Any *circularly* polarised signals would preserve their intrinsic degree of polarisation, but as has been mentioned such sources are rare and dim. Unpolarised galactic background emission would add in to reduce the overall degree of polarisation and make detection difficult. There is therefore no reason to expect the detection of extra solar system polarisation of any kind.

The cost of adding a dual polarisation capability to the VLFA is large and the benefit small. It's only use would be for solar-system work that could be done better and more cheaply using in-situ spacecraft, so on balance it cannot be recommended.

4.1.5 Overcoming the scattering limit

The above discussions have assumed that scattering defines a fundamental limit to the angular resolution of a radio telescope operating at frequencies well below 10 MHz. However, the 'image' of a strongly scattered source is *not* a smooth, quasi-Gaussian disc but rather a sequence of overlapping and rapidly changing, narrow-band speckle-patterns. In practice the observing bandwidth and integration time are such that the sum of these patterns is usually seen as a smooth disc. The question arises whether careful measurement of the pattern could be used to reconstruct an undistorted image of the radio source. The analogy is to the de-twinkling of stars by closure phase methods or the phase-correction of radio telescopes by self-calibration algorithms. Although the scattering is strong and in the far-field, there is evidence that reconstructions of this sort could be carried out if speckle measurements could be made sufficiently quickly (Cornwell 86). We will therefore consider if such measurements are feasible with the VLFA.

Plane waves shining through a thin, strongly scattering screen will give rise to a pattern of intensity fluctuations on the ground with a coherence length of $l_c = \lambda/\theta_s$, where θ_s is (again) the angular broadening of the source due to the screen. If the screen is moving perpendicular to the line of sight at a speed v_s then the speckle pattern moves over the observer at the same speed, giving a scintillation time constant of

$$\tau_s \simeq \frac{l_c}{v_s} \simeq \frac{\lambda}{\theta_s v_s} \tag{4.13}$$

By calibrating from higher frequency measurements, using $\theta_s \propto \lambda^{2.2}$, we get

Mode	τ_s
interplanetary scattering	$1.5 \times 10^{-3}\nu_{\mathrm{MHz}}^{1.2}$ seconds
interstellar scattering	$44 \times 10^{-3}\nu_{\mathrm{MHz}}^{1.2}$ seconds

Both forms of scintillation are on a time-scale of milliseconds at frequencies around 1MHz. To see the scintillation, the telescope would therefore need temporal resolution on this time-scale or better.

As well as evolving rapidly in time, the pattern is also a narrow-band phenomenon and would not be seen with a broad-band receiver. If the scattering screen is a distance z away from the observer, signals scattered from the screen at an angle θ_s interfere with the straight-through signal with a phase delay of

$$\phi \simeq \pi \frac{\nu}{c} \theta_s^2 \tag{4.14}$$

and build up a speckle pattern. A different pattern will be seen if the frequency changes by about $\Delta\nu = c/(z\theta_s^2)$, so this defines the bandwidth of the pattern. Calibrating form observations at higher frequencies we get

Mode	$\Delta\nu$
interplanetary scattering	$10\,\nu_{\mathrm{MHz}}^{4.4}$ Hz
interstellar scattering	$5 \times 10^{-9}\nu_{\mathrm{MHz}}^{4.4}$ Hz

This indicates that the scintillation bandwidth for ISS is too narrow to be measured realistically, but that interplanetary scintillation could be detected.

There is however a more fundamental limit to the measurement of scintillation. Both the bandwidth and integration time are limited by the above effects. There therefore comes a point at which the product $\tau_s\Delta\nu$ is less that 1, i.e., when no data is available for measurement. Combining Equation 4.13 with the expression for scintillation bandwidth gives

mode	$\tau_s\Delta\nu$	ν_c
IPS	$1.5 \times 10^{-2}\nu_{\mathrm{MHz}}^{5.6}$ Hz	2.12 MHz
ISS	$2.2 \times 10^{-10}\nu_{\mathrm{MHz}}^{5.6}$ Hz	53 MHz

Here ν_c is the critical frequency at which $\tau_s\Delta\nu = 1$ and corresponds to the frequency at which measurements become impossible.

It is clear from this analysis that there is no true diffractive interstellar scintillation at low frequencies and that we cannot, even in principle, remove the effects of the ISM. At frequencies above about 2 MHz however, interplanetary scintillation becomes measurable so that something could be done about the interplanetary medium. For example, interplanetary scintillation could be measured at 5 MHz using a bandwidth of < 10 kHz and an integration time of < 0.01 sec. Bandwidths even narrower should be available, as they are a natural consequence of a correlation technique that avoids the need for path compensation.

Although promising, this technique only becomes viable around the middle of the design frequency range of the VLFA where planetary observations are at their least interesting and it is likely to be computationally awkward for mapping extended structure such as the galactic background. It is therefore not recommended as a processing route unless there is some very pressing need for the slight resolution improvement it would give.

4.2. Absorption effects

One of the more important effects of the interstellar medium on observations at frequencies below about 10 MHz is the amount of energy transferred from the radiation field to the plasma via charge-separation. This is 'free-free', or 'thermal bremsstrahlung' absorption, and it makes the ionised interstellar medium optically thick (optical depth, τ, of 1) at some frequency ν_T. This turnover frequency depends on both the emission measure of the medium and its electron temperature. Specifically,

$$\nu_T = 5.21 10^{-7} T_e^{-0.64} (\underbrace{\int N_e^2 \, dx}_{\text{emissionmeasure}})^{0.48} \text{ GHz} \tag{4.15}$$

at low frequencies, where x is in parsecs along the line-of-sight. Note that this expression assumes the temperature to be constant in the region of interest. The diffuse, warm, interstellar medium has $T_e \simeq 10^4$ K and $N_e \simeq 10^5$ m^{-3}. This gives an approximate measure of the distance one can see through the medium before $\tau = 1$. As a function of frequency it is

$$l \simeq (34\nu_{\text{MHz}})^{2.1} \text{ parsec.} \tag{4.16}$$

This equation is of particular importance in both low-frequency extra-solar system planet searches and extra-galactic observations. The galactic disc has a thickness of $\sim$ 1 kpc so that the sky appears uniformly 'foggy' at frequencies below 1–2 MHz (Reynolds 90). Figure 4.4 shows an estimate for the visible optical path length through the IPM as a function of frequency, together with an indication of the median pulsar distance and the galactic diameter.

At higher frequencies however, we can see out of the plane, and the plane itself will appear mottled due to the presence of discrete regions of particularly high electron density (H II regions) absorbing the background synchrotron radiation.

At very low frequencies the free-free process absorbs much of the bright background synchrotron emission from the galaxy before it reaches us, causing the system temperature to *decrease*. Observations by the RAE-2 spacecraft predict the following antenna temperatures, T_A, as a function of observing

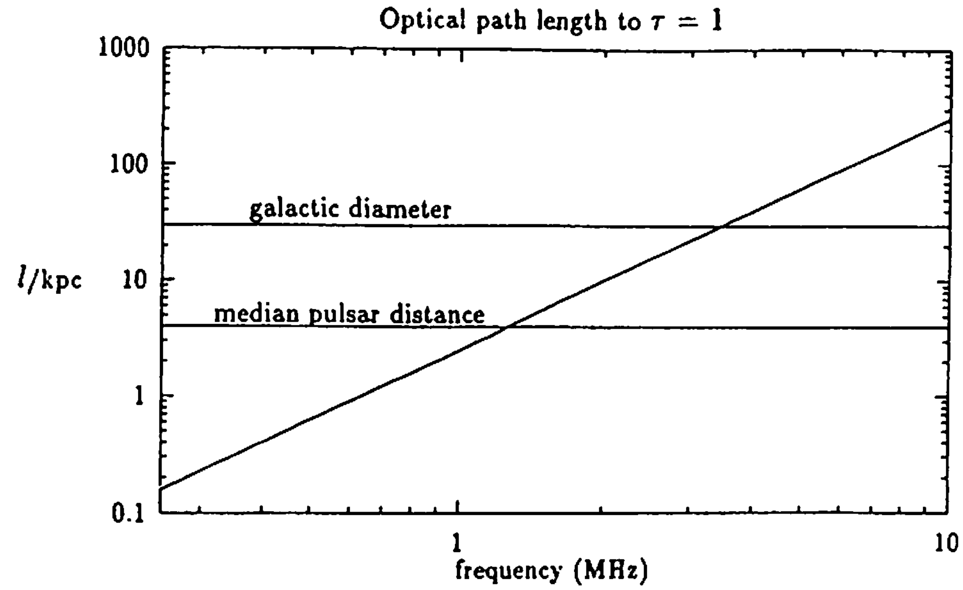

Fig. 4.4 Range of visibility through a uniform interstellar medium as a function of frequency.

frequency, ν, (Novaco 78):

T_A (K)	ν (MHz)
3.3×10^5	10
2.6×10^6	5
2.0×10^7	1
2.6×10^7	0.5
5.2×10^6	0.25

Of course, any absorption of this sort will limit the usefulness of the instrument for extra-solar system observations, both because the sky fogs over at some distance, and because the extinction will vary across the sky. This variation will give rise to uncertainties in intrinsic flux density similar to interstellar reddening seen at optical wavelengths. However, it does allow us to study in some detail the distribution of both ionised material and synchrotron emission throughout the galaxy, which is an important field in itself.

4.3. Investigating the interstellar medium

A good understanding of the interstellar medium is central to the planning and interpretation of radio observations below about 10 MHz. The effects of interstellar scattering have already been considered, but the ISM is in itself one of the major science targets for the VLFA mission.

Generally, the ionised hydrogen seen in the galaxy at low frequencies can be divided into H II regions (often seen as discrete photo-ionised clouds, mostly in the galactic plane) and warm, diffuse gas permeating the plane and extending into the halo. The denser H II regions become optically thick at about 30 MHz due to free-free absorption, whereas the diffuse emission becomes thick at 1–5 MHz (Reynolds 90). The background synchrotron emission, and the radiation from discrete background sources, is therefore seen against a complex absorption pattern generated by the ISM. This pattern is overlaid with further foreground synchrotron emission to build up an even more complex picture of absorption and emission over the sky.

One task of the VLFA is to disentangle the various components contributing to the observed temperature distribution over the sky. This process relies on both the frequency dependence of these contributions and their analysis in conjunction with ground-based observations. Although the procedure is necessarily quite involved, it is instructive at this stage to consider the major contributing effects, and determine how they might be identified and measured.

- *Galactic synchrotron emission*

As the dominant radiation mechanism in the galaxy at these frequencies, most of the radiation the VLFA detects will be galactic synchrotron emission modulated by interstellar absorption. At about 50 MHz the brightness temperature of this emission scales as $\nu^{-2.4}$. This intrinsic spectral index shows some further flattening at lower frequencies before the effects of free-free absorption increase the apparent index to about -1.3 or more at frequencies below 4 MHz. One of the goals of the VLFA will be to determine the value and distribution of the intrinsic synchrotron index over the sky as part of the investigation of the interstellar medium.

- *extra-galactic radio sources* As has already been stated, free-free emission modulates our measurements of intrinsic sky brightness and the flux densities of discrete extra-galactic radio sources. The optical depth (cf. Equation 2.1) is

$$\tau \simeq 6.5 10^5 T_e^{-1.35} \nu^{-2.1} \int N_e^2 \, dx \qquad (4.17)$$

assuming the temperature is constant through the integration path (using SI units throughout). The apparent spectral indices of sources will therefore depend on their intrinsic indices, the emission measure and the electron temperature along their line-of-sight. Each source will also show a spectral turnover at a frequency ν_T due to synchrotron self-absorption ($\nu_T \propto SB^{0.2}/\theta^2$) and the Razin-Tsytovitch effect ($\nu_T \propto N_e/B$), where B and N_e are the magnetic field and electron density local to the source, S its flux density and θ its intrinsic angular size. There are clearly many contributions to the apparent flux density of any single source, and much of the interpretation from discrete sources will therefore be statistical in nature.

Pulsars

As has already been discussed, temporal broadening prevents the VLFA from measuring pulsar dispersion, but ground-based observations at frequencies > 20 MHz are routine. The dispersion

$$\frac{\partial \tau}{\partial \nu} \propto \nu^{-3} \int N_e \, dx \, , \qquad (4.18)$$

determines the *dispersion measure* (the integral in the above equation) to the pulsar. This can be combined with the emission measure determined from free-free absorption observations to give some indication of the spatial distribution of N_e along the line-of-sight.

Optical line emission Hydrogen recombination (Hα) emission is also of great use in disentangling the various contributing factors to sky brightness. In regions of the sky that are optically thin to Hα (latitudes > 10

degrees), the emission brightness is proportional to $\int T_e^{-0.92} N_e^2 \, dx$. H$\alpha$ emission therefore also depends on emission measure but with a slightly different weighting from the electron temperature as compared to free-free absorption. The two can therefore be used for mutual verification in regions of the sky optically thin to Hα.

Although the resolution of the telescope will generally be insufficient to measure angular broadening, there should be regions of the sky where this is possible at the lower frequencies. If a sufficient number of background sources exist in these regions, the degree of broadening for each can be used to map the local ISM turbulence strength. This is similar to the approach used successfully to map density structures in the heliosphere using IPS. In principle low frequency observations of this sort are a very sensitive way of measuring weak density structures, as the angular broadening for a given turbulence strength scales as $\lambda^{11/5}$. In practice, however, it may prove difficult to detect enough background sources in the field of interest and the small variations in scattering angle may be swamped by the more powerful general structure.

4.4. Electrical properties of the Moon

A Moon-based low-frequency radio telescope has two basic advantages over one situated on the Earth. Firstly, it does not have to look through the Earth's ionosphere. Secondly, it is shielded from Earth-based radio frequency interference. This second advantage was graphically demonstrated in 1972 by the RAE2 lunar satellite, showing there to be no detectable RFI from the Earth (including auroral emission) on the far-side of the Moon. The first advantage is self evident, but it reminds us that we must consider the effects of the Moon's own atmosphere and, in particular, its ionosphere.

4.4.1 The lunar ionosphere

The Moon is known to have a tenuous atmosphere, consisting of intrinsic gaseous emission from radioactive decay (mostly ^{40}Ar), captured solar wind and material sputtered from the regolith by energetic particles. However the total mass is thought to be only about 10^4 kg (Heiken 91). Although thin, this atmosphere is still capable of having a surprisingly high plasma frequency. If we were to take the entire mass to be ionised hydrogen with a scale-height of 100 km, it would have a plasma frequency of over 12 MHz—similar to that of the Earth. The true ionised fraction and scale-height are therefore of great importance to the viability of a low-frequency instrument on the Moon's surface.

The only direct observations of the ionised component of the lunar atmosphere (other than occultation experiments from Earth) were made by the Luna 19 and 20 probes in the 1970's (Vyshov 76, Savich 76, Vyshov 79). These spacecraft made dual-frequency phase-lag measurements through the atmosphere as they orbited the Moon. By fitting these data to a model of the Moon's atmosphere, the electron density in the atmosphere can be estimated as a function of height above the lunar surface. The results vary quite widely, depending on conditions, but show densities of up to 2×10^3 cm^{-3} at altitudes of 2–10 km on the sunlit side (Figure 4.5). On the dark side of the Moon there is very little ionisation, confirming the idea that the lunar ionosphere, like that of the Earth, is photo-ionised.

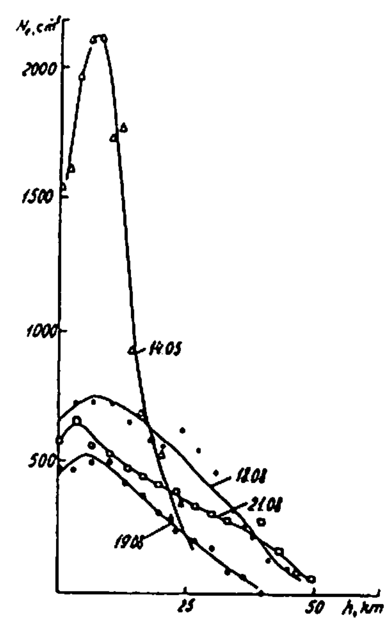

Fig. 4.5 Derived lunar ionosphere densities as a function of altitude (Luna spacecraft observations).

The densities on the sunlit side are not trivial however, and correspond to plasma frequencies of about 0.5 MHz *.

It appears therefore that, on the sunlit side of the Moon, the ionosphere could prevent measurements at frequencies below 1 MHz. Even at higher frequencies the refractive effects of the ionosphere may cause problems. Observations should therefore be carried out during the lunar night when the ionosphere is at its thinnest and the interference from solar emission is also less. It should be noted here that no reliable measurements of the ionosphere have been carried out at altitudes lower than one or two kilometers, and little has been done on the containing effects of the Moon's own weak magnetic field. A fuller understanding would clearly be needed before the construction of a lunar radio telescope.

4.4.2 The lunar regolith

The electrical properties of the surface of the Moon are of great importance in the VLFA design. Unlike the Earth, the Moon's surface has a very low electrical conductivity (about $10^{-14}\,\Omega^{-1}\mathrm{m}^{-1}$ at d.c.). This means that we may contemplate receiving the component of the electric field parallel to the surface of the Moon close to its surface. On the Earth this component is largely nulled by a strong surface reflection, π out of phase with the incident wave. Clearly, any radio source high in the sky will illuminate the Moon primarily with this component, so in practice we can expect it to be stronger than the perpendicular component. Furthermore, the receiving elements must be electrically short (at least at the longer wavelengths) so their antenna pattern will be that of a

* To a good approximation, the plasma frequency in MHz of an electron gas of density n cm^{-3} is $\nu_p \simeq \sqrt{n}/100$.

short dipole. A vertical short dipole, sensitive to the perpendicular component of the electric field, has a null at the zenith and is therefore of limited use in synthesis mapping.

If we consider a short (Hertzian) dipole parallel and close to the surface of the Moon, relative permittivity ϵ_r, the image dipole seen beneath the regolith is $-(\epsilon_r-1)/(\epsilon_r+1)$ times the real dipole in the vacuum (ignoring the imaginary component of the relative permittivity for the moment). Taking the relative permittivity of the Moon to be about 6, this image reduces the total gain in the vacuum direction to about $2/(\epsilon_r+1) = 2/7$ its free-space value (Figure 4.6).

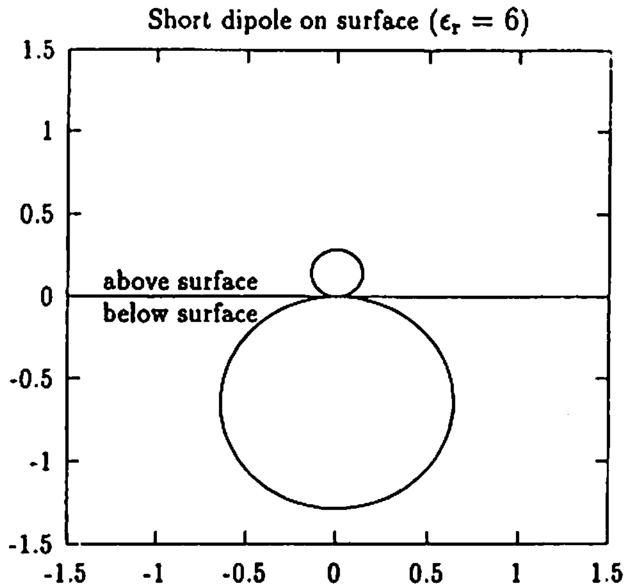

Fig. 4.6 Relative directivity of a short dipole placed horizontally on the surface of the Moon ($\epsilon_r = 6$).

Similarly, the gain beneath the surface is increased by a factor of about $(\epsilon_r + 3)/(\epsilon_r+1) = 9/7$.

The question of sensitivity will be considered later, but it is important to note at this point that, if all the system noise arises from the sky, it is the *directivity* of the antenna, rather than the gain, that determines sensitivity. Here we define gain as a measure of the power delivered into a matched load as a function of direction whereas directivity is a measure of the angular extent of the antenna beam on the sky. Hence all short dipoles in free space, matched or not, have the same directivity. Their gain on the other hand will depend on proper matching. Gain therefore has the same effect on both the signal and the noise and a change in gain will not affect the signal-to-noise ratio. The directivity determines the proportion of the field-of-view occupied by the signal source (as opposed to the noise source) and hence directly affects the signal-to-noise ratio of the instrument. This simplification breaks down when the noise from the front-end amplifiers is comparable with the voltages they are to amplify. This will occur when the forward gain of the antenna drops below some level defined by the amplifier characteristics. It seems however that a short dipole placed on the lunar surface suffers a drop in forward gain of only about 5 dB, which should be insufficient to bring the signal down to this threshold level in any practical system.

As noted above, the lobe of the dipole antenna pattern directed into the Moon is stronger than the upward lobe. This is important because any strong signals reflected from discontinuities beneath the lunar surface could be picked up by this lobe and confuse the sky observations. The relevant electrical property of the regolith to consider here is its loss tangent, L, defined as the ratio of the imaginary to the real part of its complex relative permittivity. The loss tangent, measured at between 0.001 and 0.1 during the Apollo missions (Heiken 91), gives us the skin-depth of the Moon,

$$\frac{D_s}{\lambda} = \frac{1}{\pi L \sqrt{\epsilon_r}}, \tag{4.19}$$

and hence the depth at which reflections become negligible. The skin depth, D_s, is therefore between about 1–100 wavelengths. This range allows for propagation over significant distances, particularly at the lowest frequencies, so the site should be chosen carefully to minimize the effects of sub-surface reflections.

4.5. Telescope design for an all-sky survey

At frequencies greater than 400 MHz, radio telescopes are usually designed either as survey instruments, able to cover a significant fraction of the sky at low resolution, or as high resolution instruments to be directed at specific sources. At lower frequencies the diffraction limit makes it progressively harder to construct high resolution instruments and so most telescopes operating below about 150 MHz are designed to carry out surveys. At frequencies below 10 MHz the limitations imposed by scattering in the ISM and IPM become the dominant effect, and high resolution imaging becomes impossible. A lunar low-frequency array would therefore be a survey instrument. The scattering limit is such that resolutions of a few tens of arcminutes are desirable. Furthermore, the sky background is both the dominant noise source and the primary target for mapping, so the temperature sensitivity will usually be good.

With these points in mind we should now consider the technical issues that affect the telescope design.

4.5.1 Phased array or interferometer?

One of the more fundamental design choices that must be made is whether the telescope should be a phased array of dipole elements, raster-scanning the sky beam-by-beam to build up a survey map, or an interferometer, measuring spatial scales over a large fraction of the sky all at once. Both approaches have their advantages and disadvantages, although it must be said that on Earth, most low-frequency surveys are carried out with interferometers (such as the CLFST in Cambridge, U.K.).

The data rate to the Earth from a phased array can be made very low, as some integration can be done on the Moon. A similarly low rate from an interferometer requires the correlator to be either on the Moon's surface or in close orbit. A phased array also has slightly better sensitivity than an interferometer, but it is basically a power-measuring telescope, so interference always adds positively, no matter where it is in the beam. An interferometer on the other hand is less sensitive to interference, particularly if the source moves through the beam, as the signals add either positively or negatively, depending on the sign of the lobe the source is in. In both cases the beams rotate on the sky over long integration periods. However the mean side-lobe levels of a phased array, averaged over the rotation, are those of the mean square voltage pattern, whereas an interferometer gives the square of the mean voltage pattern. We can therefore expect the side-lobes to be lower in a map made with an interferometer.

Conventionally, both phased arrays and interferometers need path compensation. This represents one of the more difficult design features to implement electronically in any telescope as the delays involved are often very small (~nanoseconds). On Earth these delays are usually generated by inserting appropriate lengths of cable into the signal path. On the Moon this solution is unattractive, as the weight of the cabling needed would be prohibitive. We can however remove the need for path compensation if we work with sufficiently narrow bandwidths. In this way the 'white light' fringe condition is maintained naturally. Roughly, if we wish to map a region of sky of angular width θ_v using a baseline (or array size) of L without path compensation, the bandwidth used must be

$$\Delta\nu < \frac{c}{L\theta_v}\,. \tag{4.20}$$

A practical scheme would involve dividing up the total observing bandwidth at each antenna into many narrow sub-bands (see below), probably by using digital signal processing chips. The antenna sub-bands are then either summed with the correct phase to point the telescope in the desired direction (phased array) or separately correlated to produce many narrow-band maps which can be co-added (interferometer).

This scheme falls more naturally into an interferometer design, which already requires considerable digital processing, than into a phased array design, which is potentially less reliant on digital techniques. However, to get the *full* benefit of a phased array telescope, one would have to generate many phased beams on the sky simultaneously (so generating the equivalent of a focal-plane array at the focus of big dish). This would itself require a considerable amount of Moon-based electronics so the apparent simplicity of the phased-array approach is lost.

Interstellar temporal broadening is sufficiently great for there to be essentially no source variability at these frequencies, so the time needed for synthetic aperture interferometric mapping need not be a limitation. Furthermore, if we put the correlator on the Moon or in lunar orbit, the high data-rate from an interferometer ceases to be an issue and the post-correlation data rate can be made as low as that from a phased array.

It should be noted that the digital design for the telescope as outlined above is sufficiently flexible for the decision between the two competing designs to be one made in the DSP software rather than the telescope hardware. To avoid the need for path compensation, both designs require the signals from each antenna to be mixed to base band, digitised and then split into many sub-bands by an FFT chip. These sub-bands are then passed to a DSP block, situated close to the centroid of the antennas, which combines the digital signals to produce beams on the sky that are either 'point-like' (the phased array) or 'wave-like' (the interferometer). The distinction is not as severe as it seems at first. Probably the most important distinction between the two appears only when we consider the rotation of the Moon and the effect of this rotation on the mean beam shape. The beam shape is better when we configure the telescope as an interferometer, so from this point onward we will consider only the needs of the interferometer.

4.5.2 Field-of-view considerations

The telescope's field-of-view is limited by the presence of the Moon cutting out approximately 2π steradians of sky at any one time. The receiving elements themselves are electrically short. Although they carry a dipole anisotropy they will receive signals from practically all the visible sky simultaneously. As described above, the field of view of the whole telescope is therefore defined by chromatic effects. For an interferometer this is known as 'bandwidth smearing', and is caused by the dependence on wavelength of both the resolution and size of the map. Loosely, Equation 4.20 shows that to make an $n \times n$ pixel map, the fractional bandwidth used must be

$$\frac{\Delta\nu}{\nu} \leq \frac{1}{n}. \tag{4.21}$$

To take an example, a synthesis map made by a telescope on the Moon's equator covering the whole sky with a resolution of 0.25 degrees would have a value of $n \simeq 800$. If the observing frequency were 1 MHz, the bandwidth of each sub-channel would therefore have to be ~ 1 kHz. This would mean that a map of the sky made at 1 MHz with a total bandwidth of 100 kHz would in fact consist of about 100 narrow-band maps added together. In practice, this addition occurs most naturally in the aperture plane immediately after correlation and before the final mapping transform.

4.5.3 Processing power

As will be shown below, the lunar telescope will need about 300 elements but will have an instantaneous bandwidth of only about 100 kHz. The total data rate is therefore high, but it is distributed over many channels. This allows us to consider a fully digital design for the correlator. As has already been stated, path compensation can be side-stepped if the data from each antenna are divided into a great many ($\sim$ 100) sub-bands before correlation. This can best be done digitally using specific FFT chips or more general digital signal processing (DSP) chips. Once digitised, the correlation is then naturally carried out digitally. The amount of processing power required to handle all the data from the telescope must therefore be estimated. Assuming there are 300 elements in the interferometer, each measuring two polarisations (possibly the worst case), the number of real correlations to be carried out in each band is

$$N_{\rm corr} = \underbrace{\frac{1}{2} \times 300 \times 299}_{\rm No.of baselines} \times \overbrace{2}^{\rm sin\&cos} \times \underbrace{2}_{\rm polarisations} = 179,400\,. \tag{4.22}$$

In terms of the number of floating point operations per second (flops) there is no overhead in dividing the full bandwidth into many sub-bands because the data rate in each is proportionately less. If we assume a full bandwidth of 100 kHz, the processing power necessary to correlate all available baselines is therefore about 3.6×10^{10} flops. Although this appears a fearsome figure, the task can be distributed efficiently between a number of processors. Even with present day technology, using chips from the inexpensive Analog Devices ADSP-2100 family, an array of about 1000 processors would be sufficient.

4.5.4 Flux sensitivity

The telescope can be used to detect unresolved or resolved sources. The sensitivity of the instrument to radiation from an unresolved source is defined by its flux sensitivity. The sensitivity to a resolved source (i.e., a source larger than the synthesised beam) is defined by its brightness temperature sensitivity, or flux sensitivity per unit solid angle.

In both cases the noise that limits the sensitivity should be dominated by emission from the sky, which is at temperatures of up to 10^7 K at these frequencies*, rather than the receiver electronics. This is an important design criterion for the dipole/front-end sub-system. The radiation resistance of a short dipole is about

$$R_r \simeq 20\pi^2 l^2/\lambda^2 \,, \tag{4.23}$$

so at 1 MHz, a 10 m antenna has a radiation resistance of 0.2 Ω. Matching to such a small resistance is difficult but can be overcome if we realise that, as both the noise and the signal come from the antenna, there is no need for efficient power transfer between the antenna and the preamplifier. The preamplifier can therefore have a high input impedance so that the antenna simply acts as a probe of the electric field, developing a potential difference over its ends of $V \simeq El$ where E is the electric field and l the length of the dipole. Assuming this voltage can be amplified without introducing further noise, the telescope will see a 'bright' sky, the brightness of which will vary somewhat from point to point. It is this brightness variation, caused by differences in both synchrotron emission and interstellar absorption, that the telescope must map. Discrete sources will be seen within this brightness distribution so measurement of individual flux densities will be contaminated by uncertainties in the point-to-point variance of background emission.

Because the noise contribution is 'self-noise' from the structures we wish to map, the sensitivity of the instrument is very high. Indeed, if we were to use a fully-filled phased array, the signal-to-noise ratio per beam area would be

$$\mathrm{SNR} = \sqrt{\Delta\nu\tau} \,, \tag{4.24}$$

where $\Delta\nu$ is the full bandwidth and τ the integration time per beam. A multi-beam array covering the whole sky to the desired resolution would therefore reach a signal-to-noise ratio of 100 with a bandwidth of 100 kHz in 0.1 seconds! More realistically, we cannot attain a resolution of 0.25 degrees with a fully filled aperture as the number of individual elements would be prohibitively high, so the sensitivity will be correspondingly lower.

Generally, the flux sensitivity of an n element interferometer ($n \gg 1$) is

$$\Delta S = \frac{2kT_{\rm sys}}{nA_{\rm eff}\sqrt{\Delta\nu\tau}} \,, \tag{4.25}$$

where $A_{\rm eff}$ is the effective area of a single element, $T_{\rm sys}$ the system temperature, $\Delta\nu$ the total observing bandwidth and τ the observing period. The effective area in this expression represents the directivity of the antenna elements. For a short dipole

$$A_{\rm eff} = \frac{3}{2}\frac{\lambda^2}{4\pi} \tag{4.26}$$

* The sky brightness is about 12 Jy per 1/4 × 1/4 degree beam at 1 MHz

so the flux sensitivity of the interferometer is

$$\Delta S = \frac{16kT_{sys}}{3n\lambda^2\sqrt{\Delta\nu\tau}}. \tag{4.27}$$

A power-law fit to the galactic spectrum seen by RAE below 4 MHz gives $T_{sys} = 10750\lambda^{1.324}$. The flux sensitivity in Janskys then becomes

$$\Delta S_{Jy} = 5.3 \times 10^6 \frac{\nu_{MHz}^{0.676}}{n\sqrt{\Delta\nu\tau}}. \tag{4.28}$$

As an example, taking $n = 300$, $\Delta\nu = 10^5$ Hz and $\tau = 1.3 \times 10^6$ seconds (15 days) the flux sensitivity is 0.05 Jy. Although probably insufficient to detect emissions from an extra-solar-system planet, this sensitivity is sufficient to map the sky background (which at 1 MHz has a surface brightness of about 12 Jy beam^{-1} at a resolution of 0.25 degrees) with a signal-to-noise ratio of about 200. This is effectively the temperature sensitivity of the telescope—a result that will now be demonstrated more directly.

4.5.5 Temperature sensitivity

The temperature sensitivity of the telescope is of greater importance than its flux sensitivity. This is because the resolution of the instrument will be at or slightly below the angular broadening limit set by scattering, and most of the observations will therefore be of 'resolved' structures, broadened to more than one pixel.

The temperature sensitivity can be derived directly from the flux sensitivity, defined by Equation 4.25. The flux density from a region of the sky of solid angle Ω and temperature T is defined as

$$S = 2kT\Omega/\lambda^2. \tag{4.29}$$

If the sky is imaged with a maximum baseline of D, then $\Omega \simeq (D/\lambda)^2$. Combining this with the previous equation and Equation 4.25 gives a temperature sensitivity of

$$\Delta T = \frac{D^2 T_{sys}}{nA_{eff}\sqrt{\Delta\nu\tau}}, \tag{4.30}$$

and a signal-to-noise ratio in temperature of

$$\text{SNR} = \frac{T_{sys}}{\Delta T} = f\sqrt{\Delta\nu\tau}. \tag{4.31}$$

The factor f equals nA_{eff}/D^2 and is the *filling factor* of the interferometer—literally the fraction of the synthesised aperture actually filled by real antennas at any one moment. It is this factor that drops the temperature sensitivity well below the theoretical figure derived for a fully-filled aperture at the beginning of this section. If we take $n = 300$, $\nu = 1$ MHz and D = 70 km (0.25 degree resolution) we get $f \simeq 6.6 \times 10^{-4}$. Clearly most of our aperture is missing. The temperature signal-to-noise ratio after a 15-day integration at 1 MHz with a bandwidth of 100 kHz is therefore about 200.

A signal-to-noise ratio of 200 is quite sufficient to do most of the astronomy we require. Indeed, uncertainties in the side-lobe levels may prevent useful observations being made with greater finesse than this. Thus a 300-element interferometer operating at 1 MHz placed near the lunar equator can map the entire visible sky by rotation aperture synthesis in half a lunar day. A practical observing program would involve many such maps being made at spot frequencies throughout the design frequency range of the instrument.

The filling factor for short dipoles scales as λ^2, so that at 10 MHz it is 100 times less than at 1 MHz. The system described above would therefore have a signal-to-noise ratio of only 2 at 10 MHz—insufficient for practical work. This figure may be improved by

- Only using an inner 'sub-array' for the higher frequencies. This array would need to have fewer antennas but a larger filling factor. The angular resolution would then be limited to less than that available with a 70 km baseline (1.5 arcminute) but the temperature sensitivity would recover.
- Increasing the observing bandwidth at the higher frequency.
- Observing the sky for more than one night.

Part of the solution to this problem is therefore to be found in optimally positioning the antennas.

4.5.6 Relative antenna positions

The subject of antenna placement is a particularly subtle part of any interferometer design. In the case of the VLFA it is further complicated by the need for a wide range of operating frequencies and the strong dependence of filling factor (and hence sensitivity) on wavelength described above. The optimum solution must wait for its own design study, but some general points can be made straightaway.

The individual antennas in the instrument are dipoles and respond well to signals from practically anywhere on the sky. These elements have no real primary beam so strong sources are limited only by the synthesised beam, the side-lobes of which should be kept as low as possible. For a fixed number of antennas, the power in these side-lobes is minimised when the baselines are non-redundant, making a non-redundant configuration particularly attractive.

To continue the design, two conflicting criteria must be balanced:

- The quality of the map is improved if the interferometer samples the transform plane uniformly, so measuring all spatial scales in the sky brightness distribution.
- The temperature sensitivity of the telescope depends on the filling factor, which, because we are using short dipoles, drops as λ^2. We can only recover sensitivity at the higher frequencies (and the same resolution) if the filling factor for the shorter baselines is greater than that for the larger baselines.

Some of the antennas must contribute only to the larger spacings so they can be excluded at higher frequencies. This makes the array smaller, and allows us to attain at higher frequencies a filling factor similar to that attainable at lower frequencies. Clearly, the antennas cannot be arranged with uniform density as this would not allow us to improve the filling factor by excluding the outer ones. Rather, the space-density of the antennas must drop off, possibly rapidly, as we move out from the centre. This introduces a notional 'inner' and 'outer' array into the design. The two arrays are used together in the lower portion of the frequency range to get maximum resolution. The outer array, containing fewer antennas, is not used for higher frequency observations. At these frequencies the inner array alone has a better filling factor and can map the sky at a similar resolution.

The classic 'Y'-shaped design, used for the VLA and other telescopes, embodies many of these features. The antennas are spaced logarithmically along the three arms such that the distance to the ith antenna is proportional to i^{α} ($\alpha \geq 1$). In this way, spatial scales are measured similarly over a wide range of observing frequencies, and the filling factor for the inner antennas alone is greater than the filling factor of the whole.

It is difficult to use a simple 'Y'-shaped design for the VLFA because, with 300 antennas in total, there is insufficient space in the inner zone. A practical design would include antennas spread more evenly around the vertical axis of the array in this inner zone, resolving to a classic 'Y' only in the more distant reaches.

If there are n antennas in total, we can define an antenna density function by

$$\rho(\vec{r}) = A_{\rm eff} \sum_{i=1}^{n} \delta(\vec{r} - \vec{r}_i)\,, \tag{4.32}$$

where $\vec{r}_i$ is the position vector of the ith antenna relative to the telescope center. The filling factor of the array, out to a distance R from the center, is then

$$f(R) = \frac{A_{\rm eff} \int^{|\vec{r}| \leq R} \rho(\vec{r})\, d^2r}{\pi R^2}\,. \tag{4.33}$$

We can now compare the sensitivity of the instrument at different frequencies by fixing the resolution at $\theta_{\rm r}$ and only using antennas out to $R = \lambda/(2\theta_{\rm r})$. Taking $A_{\rm eff} = 3\pi\lambda^2/8$ gives a total filling factor as a function of wavelength of

$$f_\lambda = \frac{3}{2}\theta_{\rm r}^2 \int^{|\vec{r}| \leq \lambda/(2\theta_{\rm r})} \rho(\vec{r})\, d^2r\,. \tag{4.34}$$

The optimal positions of the antennas, $\vec{r}_i$, are the ones that maximise the above expression and minimise the power in the side-lobes of the synthesised beam over the design frequency range *. The calculation must also take account of the relative proximity of antennas. If closer than about a wavelength they do not contribute independently to the filling factor and must be taken together. The procedure is not trivial, but the optimisation strategy is well defined.

4.5.7 Summary of the telescope design

When mapping the sky at these frequencies we may assume that the system temperature is due solely to the noise arriving in through the antenna. We can therefore ignore noise contributions from the electronics themselves. The design of the front-end is crucial, as an insensitive design may result in the receiver temperature exceeding the contribution from the sky, so disallowing this assumption.

The resolution of the sky survey is limited by scattering to a few tens of arcminutes, so it is more useful to think in terms of brightness temperature sensitivity (i.e., a measure of flux per unit solid angle) than flux sensitivity. All the system noise is assumed to be due to the sky, so the expression for the signal-to-noise ratio in the map is particularly simple, and reduces to

$$\mathrm{SNR} = f\sqrt{\Delta\nu\tau}, \tag{4.35}$$

where $\Delta\nu$ is the observing bandwidth, τ the integration time and f the filling factor of the synthesis array. The filling factor is defined as the ratio of the total physical collecting area of the elements to the area of the synthesised aperture.

* the instantaneous synthesised beam is the Fourier transform of the auto-correlation of $\rho(\vec{r})$.

Taking the maximum baseline of the array to be D, the synthesised aperture has an area of $\simeq D^2$. If we assume the receiving elements are electrically short dipoles spaced sufficiently far apart that they do not interfere with each other (i.e., $> \lambda$) they each have an effective collecting area of

$$A_{\text{dipole}} = \frac{3}{2}\frac{\lambda^2}{4\pi}. \tag{4.36}$$

It is helpful to note that the concept of 'collecting area' is used here to reflect the extent of the beam pattern on the sky rather than the efficiency of the antenna at absorbing energy. The ratio of these two areas gives the filling factor

$$f = n\frac{3}{8\pi}\left(\frac{\lambda}{D}\right)^2, \tag{4.37}$$

where n is the number of dipole elements deployed in the array.

Finally therefore, the signal-to-noise ratio for the telescope becomes

$$\text{SNR} = n\frac{3}{8\pi}\frac{\lambda^2}{D^2}\sqrt{\Delta\nu\tau}. \tag{4.38}$$

If we take as an example $\lambda = 300$ m (1 MHz), $\Delta\nu = 100$ kHz, $\tau = 1.2 \times 10^6$ seconds (14 days) and $D = 70$ km we get a signal-to-noise ratio of $SNR \simeq 0.76n$. A choice of $n = 300$ therefore results in a perfectly acceptable signal-to-noise ratio of 228.

The all-sky survey could therefore be completed in one lunar night. Any proper survey would then go on to repeat the measurements at a number of spot frequencies throughout the design range of the telescope. A suitable number might be 20 frequencies, spaced logarithmically between 0.5 and 10 MHz.

It is important to consider how the n antennas are to be arranged within the boundary of the synthesised aperture. Clearly, the best filling factors are achieved when the elements are in a close-packed configuration, literally 'filling' the synthesised aperture. In the case of the VLFA though, there are insufficient antennas to achieve this, and other configurations must be considered. Arrangements that perform well in 'snap-shot' mode are of lesser interest as the instrument will almost always be operating as a rotation synthesis telescope. A classic 'Y'-shaped configuration is attractive, with further antennas placed around the centre to increase the inner filling factor. The filling factor of the telescope taken as a whole drops as ν^{-2}, so at higher frequencies this 'inner' array can be used on its own without reducing the angular resolution below the level attainable at lower frequencies.

4.6. Overall summary

We see from the above that there are a number of important effects that must be considered and balanced in the design of a lunar radio telescope operating at very low frequencies. One of the driving forces behind such a telescope is the need to get above the Earth's own ionosphere, which is largely opaque to radio waves at frequencies below 10 MHz. What we are left to contend with is a residual lunar ionosphere, which has a plasma frequency well below 0.5 MHz during the lunar night, the interplanetary medium and the interstellar medium.

The lunar ionosphere can be neglected if we observe only when the Sun is below the horizon, but the IPM and ISM will always be present. Their main effect is to broaden the apparent angular sizes of sources to discs of around 1 degree at 1 MHz, so limiting the effective angular resolution of the instrument. Although it may be possible to remove some of the effects of the IPM using scintillation techniques those from the ISM are irreversible.

The scattering also limits the temporal resolution of the instrument. This is severe enough for it to be impossible to detect pulsed emission from nearly all known pulsars and to reduce the instruments sensitivity to transient signals (< 1 s) in the solar system at frequencies below 600 kHz.

One of the clearest signatures we expect to see with the VLFA is that of free-free absorption in the ISM. This has the effect of dimming both the synchrotron background radiation and signals from discrete sources. The amount of extinction in a particular direction depends on the emission measure and this will vary both within the galactic plane and out of it. At frequencies below 1–2 MHz we can expect the sky to appear almost uniformly foggy. At higher frequencies the absorption will give the background emission a more 'blotchy' appearance. The study of these effects gives important information on both the ISM and the Galaxy's synchrotron background radiation and is a primary goal of the mission.

The antennas themselves will be electrically short ($l \ll \lambda$) and can be laid flat on the Moon's surface. This skews the gain pattern so that the antennas are more sensitive to signals coming up from beneath the surface, but careful placement should ensure that nearly all the signal received comes directly from the sky.

The antennas must be arranged in a fixed configuration giving good sensitivity over a wide range in frequencies. The most promising type of design appears to be one similar to the classic 'Y' shape but with extra antennas in the inner zone to increase the filling factor there. Such an instrument, operated as an interferometer, should have sufficient temperature sensitivity to map the whole sky with a resolution of 0.25 degrees in half a lunar day, assuming a bandwidth of 100 kHz. The correlator used for this should be digital in design and make heavy use of DSP techniques. In particular, by dividing the observing bandwidth into many narrower sub-bands the need for path compensation can be removed.

References

Duric, N., and J.O. Burns, Very low frequency radio astronomy from lunar orbit, Engineering, Construction and Operations in Space, IV, Proceedings of Space, 94, vol 2, edited by G. Galloway and S. Lokaj, 19??.

Weiler, K.W., B.K. Dennison, K.J. Johnston, R.S. Simon, W.C. Erickson, M.L. Kaiser, H.V. Cane, M.D. Desch, and L.M. Hammarstrom, A low frequency radio array for space, Astron. Astrophys., 195, 372-379, 1988.

Cordes, J.M., Pidwerbetsky, A., & Lovelace, R.V., 1986, *Ap. J.*, **310**, 737.

Cordes, J.M., 1990, *Low Frequency Astrophysics from Space*, eds. Kassim, N.E., & Weiler, K.W., Springer Verlag Lecture Notes in Physics No. 362, p. 165.

Cornwell, T.J., & Napier, P.J., 1986, *Radio Astronomy from Space*, ed. Weiler, K.W., Proc. of NRAO Workshop No. 18, p. 215.

Erickson, W.C., 1964, *Ap. J.*, **139**, 1290.

Heiken, G.H., Vaniman, D.T., & Bevan, M.F., 1991, eds., *The Lunar Source Book*, Cambridge University Press, p. 40.

Novaco, J.C., & Brown, L.W., 1978, *Ap. J.*, **221**, 114.

Reynolds, R.J., 1990, *Low Frequency Astrophysics from Space*, eds. Kassim, N.E., & Weiler, K.W., Springer Verlag Lecture Notes in Physics No. 362, p. 121.

Rickett, B.J., 1977, *Ann. Rev. Astron. Astrophys.*, **15**, 147.

Savich, N.A., 1976, *Space Research XVI*; Proc. of Open Meetings of Workshop Groups on Physical Sciences, Akademie-Verlag, p. 941.

Tribble, P.C., 1991, *Mon. Not. R. Astr. Soc.*, **250**, 726.

Vyshov, A.S., 1976, *Space Research XVI*; Proc. of Open Meetings of Workshop Groups on Physical Sciences, Akademie-Verlag, p 945.

Vyshov, A.S., & Savich, N.A., 1979, *Cosmic Research*, **16**, 450.

5

BASELINE SPECIFICATIONS

The specification for the VLFA observatory is driven by the characteristics of the sky in this frequency band, as far as they are known to us at present. The low-frequency radio emissions from distant sources will be scattered by the intervening turbulent plasma, notably the interplanetary medium and the interstellar medium. This has the effect of smearing the signals both spatially and temporally as well as distorting their polarisation. Very little observational data is available in this frequency band with significant spatial resolution. This has lead to the first priority of the proposed observatory to be an all sky survey in the frequency band 500 kHz to 16 MHz. Because the solar system emissions will only be affected by the interplanetary medium, a separate receiver system is proposed for these objects. This receiver system can be optimised for the higher signal strength and time variability of these signals.

5.1. All sky survey

For sources subject to interstellar scattering, the temporal broadening at 1 MHz is approximately equal to the proposed mission lifetime of 5 years. We can therefore relax the requirements on the time to map the sky and concentrate on observing the sky in a narrow bandwidth of 100 kHz at a time. A map of the sky over the frequency range 500 kHz to 16 MHz should then be easily achievable over the mission duration if we have a sensitivity sufficient to map a 100 kHz band in less than one lunar night.

The resolution of the sky survey in this bandwidth is limited by scattering to a few tens of arcminutes. We have therefore chosen the VLFA to have a minimum resolution of 0.5 degree at 1 MHz.

Although polarisation will be significantly modified by the interstellar medium, it is recommended that the array shall separately record left and right hand polarised intensities.

As it is likely that interference will be recorded , it is proposed that all data from the array shall be collected in time bins and time tagged with an absolute accuracy of better than 1 millisecond. This will allow the elimination of poor quality data prior to generating the map.

It should be possible to place the array on the lunar surface at a latitude that will give a coverage of more than 60% of the celestial sphere over the 5 year mission duration.

A summary of these requirements is given in Table 5.1.

Table 5.1 All sky survey requirements

Frequency range	500 kHz to 16 MHz
Instantaneous observing bandwidth	100 kHz
Spatial resolution at 1 MHz	0.5 °
Time to generate one map	300 hrs
polarisation	left and right
Data time tag	1 ms
Sky coverage	> 60%

5.2. Solar system receiver requirements

The solar system receiver has a quite different set of requirements to allow efficient measurement of solar system objects. Its implementation may be quite separate from the all sky survey array although resources may be common.

To cover the known low frequency planetary emissions and to have some overlap with ground observations the Solar system receiver shall be capable of operating from 100 kHz to 30 MHz. The low band range from 100 kHz to 2MHz is proposed to be divided into 200 frequencies bands and the high band range from 2 MHz to 30 MHz into 300 frequency bands.

It is proposed that all 500 frequencies shall be simultaneously measurable with a time resolution of 1 second in both right and left polarisation. A higher time resolution of 5-10 milliseconds is also desirable when measuring a limited number of 20 fixed frequencies.

As the solar system sources generating these signals are generally known, no spatial resolution is needed for these observations.

The receiver should be able to detect flux densities of 10^{-21}W/m^{2}Hz at 250 kHz and to allow the sense of polarisation (left-handed or right-handed) to be detected.

As for the all sky survey instrument, all data from the Solar System Receiver shall be time tagged with an absolute accuracy of better than 1 millisecond.

A summary of these requirements is given in table Table 5.2.

Table 5.2 Solar system observation requirements

Frequency range 500 kHz to 2 MHz	200 bands
Frequency range	2 MHz to 30 MHz 300 bands
Time resolution (500 band mode)	1 s
Time resolution (20 band mode)	10 ms
Spatial resolution	none
polarisation	left and right
Sensitivity	10^{-21}Wm^{-2}Hz^{-1}
Data time tag	1 ms

6

A STRAWMAN DESIGN

6.1. Array configuration

The temperature sensitivity of the array is largely defined by its filling factor, f. Normally the filling factor of a telescope is not affected by the observing frequency. However, because the VLFA uses short dipole antennas, the effective area of which scales as λ^2, the filling factor of the array also scales as λ^2. At 1 MHz ($\lambda = 300$ m) the effective area of the antenna is sufficient for signal-to-noise ratios of about 200 to be achieved with an angular resolution of 0.25 degrees. At higher frequencies, however, the filling factor drops rapidly (assuming the whole array is used to its maximum resolution).

The signal-to-noise ratio at higher frequencies can be recovered if we limit the size of the synthesised aperture by omitting the longer spacings. In this way we reduce the resolution of the array below that achievable from the whole configuration, but gain sensitivity per map pixel. We therefore imagine a configuration with outer antennas used solely at the lower frequencies but inner antennas used at all frequencies. A useful design consideration is to state that the telescope should adapt so as to map the sky *with the same angular resolution at all frequencies.*

One obvious approach is to use a Y-shaped design similar to that employed in the VLA. Each of the three arms then holds, say, 100 antennas and the antennas are spaced along the arms in a power law, so that the distance from the origin to the ith antenna is

$$d_i = Ai^{\alpha} \tag{6.1}$$

where A and α are constants. If $\alpha = 1$ we have a uniformly spaced line of antennas. This is a highly redundant configuration, giving poor baseline coverage and hence a poor beam. In the VLA an index of 1.7 is used, so for simplicity we will consider the same index. One advantage of a power law design such as this is that the beam shape can be made the same at all frequencies—a point we will return to later.

To get a maximum baseline of $D_{\max}$ in the array, the arms must be $D_{\max}/\sqrt{3}$ long. We therefore need arms of about 40 km to get a resolution of 0.25 degrees at 1 MHz. As we need to fit 100 antennas along each arm, it follows that

$$A = 40/(100^{1.7}) = 0.0159 \tag{6.2}$$

This constraint therefore defines the exact form of the antenna distribution. Unfortunately though, many of the inner antennas are rather close together in this design. Indeed, the distance between the antennas is less than 300 metres for the inner 1/3 of all the antennas. The need is for a modified design that allows more space between the inner antennas, while still retaining a Y-shaped format for the longer spacings.

6.2. Spiral configuration

We will now consider a simple modification to the Y-shaped power law design considered above that takes care of the need for greater space between adjacent elements in the inner zone. If the arms of the array spiral around the vertical axis as they approach the centre we can increase the effective length of the arms without increasing the overall extent of the array. This extra 'length' allows for a larger value for A and hence greater antenna separation along the arm. The main disadvantage of this approach is that the array no longer scales simply with frequency as the pitch of the spiral introduces a scale-length into the design. It does however retain the simplicity of just three arms, which aids deployment.

If the array is to spiral towards the centre, the position angle of an antenna relative to the north-south line on the lunar surface must depend on its distance from the origin, i.e., $\theta = \theta(r)$. If we define the length of a spiral track within a radius R as $L(R)$ we have

$$L(R) = \int_0^R \sqrt{1 + r^2 \left(\frac{\partial \theta(r)}{\partial r}\right)^2} \, dr \tag{6.3}$$

The number of antennas contained within a circle of radius R is therefore

$$n(R) = L(R)^{-\alpha} \tag{6.4}$$

A suitable choice for the form of the function $\theta(r)$ is one that drops to zero for large r, so that the array resolves to a simple 'Y' in its outer reaches. We will use an exponential function for this, so that

$$\theta(r) = P \exp(-\beta r) \, , \tag{6.5}$$

where β defines the distance from the origin at which the spiralling becomes weak, and P defines the strength of the spiral, i.e., the number of turns the track undergoes in some radial interval r.

No attempt has been made to optimise the design parameters used here. Rather, we present in Table 6.1parameters that are *sufficiently good* to fulfil our sensitivity requirements over the observing bands considered.

Table 6.1 Spiral parameters

α	1.7
β	0.25
P	16

These parameters give an array with a design angular resolution of 0.25 degrees enclosed within a circle of radius 39.7 km. The maximum baseline available is 68.75 km and each spiral arm has a length of 86.12 km. The arrangement of antennas in this array is shown in Figure 6.1.

Figure 6.2shows the number of antennas enclosed within a circle of radius $R(R < 39.7\text{km})$ for the design.

This figure is important because the number of antennas enclosed for a given resolution is proportional to the filling factor, and hence the sensitivity. To see this, remember that $f = nA_{\text{eff}}/(\pi R_{\text{max}}^2)$, and that the effective area of

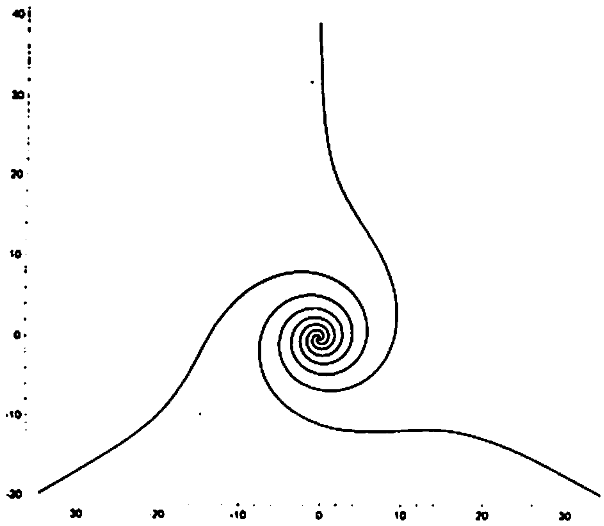

Fig. 6.1 Spiral array configuration

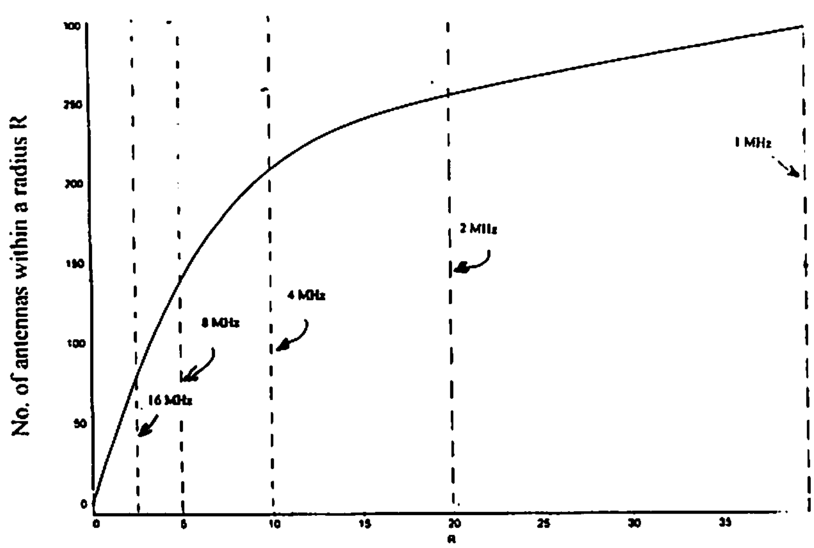

Fig. 6.2 Number of antennas within a given radius R

a short dipole is $A_{\text{eff}} = 3\lambda^2/(8\pi)$. If we define our angular resolution to be $\Theta_r = \lambda/D_{\text{max}}$, then the filling factor reduces to

$$f = \frac{9n\Theta_r^2}{8\pi^2} \tag{6.6}$$

which is independent of λ but does depend on n, the number of antennas within the circle of radius R_{max} defined by the chosen resolution ($R_{\text{max}} = \lambda/(\Theta_r\sqrt{3})$). Our chosen integration time and bandwidth give a signal-to-noise ratio of

$$\text{SNR} \simeq 2n/3 \tag{6.7}$$

The graph can now be used to determine the signal-to-noise ratios for our range of frequencies. Lines are drawn on to show the number of antennas used for observing frequencies of 1, 2, 4, 8, and 16 MHz. The signal-to-noise ratios for these frequencies are approximately

Table 6.2 Signal to noise ratio

Frequency (MHz)	n	SNR
1	300	200
2	252	168
4	208	139
8	135	90
16	80	53

The configuration therefore maintains a reasonable signal-to-noise ratio up to the maximum design frequency.

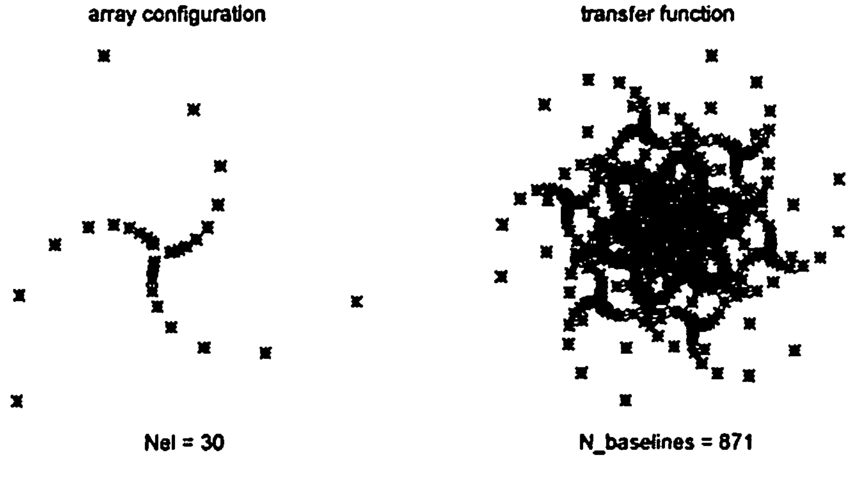

Fig. 6.3 uv-plane coverage

6.3. Data processing and communication

Independently of the data processing and communication scheme selected, a relay satellite in view of both the moon far side and the earth is needed to transmit data and commands. Our solution consists in placing the relay satellite in a halo orbit around 2^{nd} Lagrange point of the earth-moon system (Figure 6.4). This minimises tracking requirements and permits continuous link.

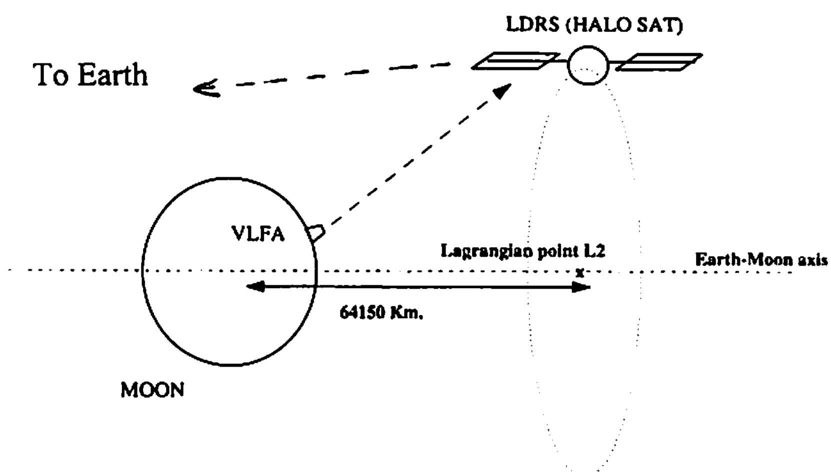

Fig. 6.4 Earth-Moon communication scheme

We then investigated several data processing and communication schemes, namely

- direct link between each receiver element and the earth, with correlation done on earth,
- direct link between each receiver element and a central station and transmission of the raw data to earth
- direct link between each receiver element and a central station where correlation is performed prior to transmission to earth,
- variations of this last solution using repeaters to reduce the height of the central station antenna (for direct line of sight link), or using each receivers as repeater in a daisy chain mode.

We concluded that the most efficient and reliable solution consists in using a central station where the data is correlated, and in using a small number of repeaters to minimise the central station antenna height. The general scheme is shown in Figure 6.4 and uses 3 repeaters for each array branch to compensate for lunar curvature.

The data rate from each receiver is 800 kbs (2 bits per sampling $\times$ 200 samples per second $\times$ 2 polarisations). The transmission to the central station is done over a carrier at 15 GHz, a frequency which minimises the size of the receiver horn antennas and is compatible with Recommendation 479-3 of the CCIR on "Protection of frequencies for radio astronomy measurements in the shielded zone of the moon".

After correlation at the central station, the data volume is 3.19 kb/s [$2N(N-1)/2 = 89,700$ correlations × 16 levels × 2 polarisations / 900 s integration time], a rate which is easily handled by traditional satellite communication systems.

6.4. Receiver elements

6.4.1 Antenna

The equivalent circuit of a short dipole consists of a low value resistance The dipole dimensions have been mainly determined by structural and mass considerations. However, the study concluded that the specifications were met with a dipole of 4m in length, an outer radius at dipole centre of 2cm, and thickness of 0.25 mm (Figure 6.5).

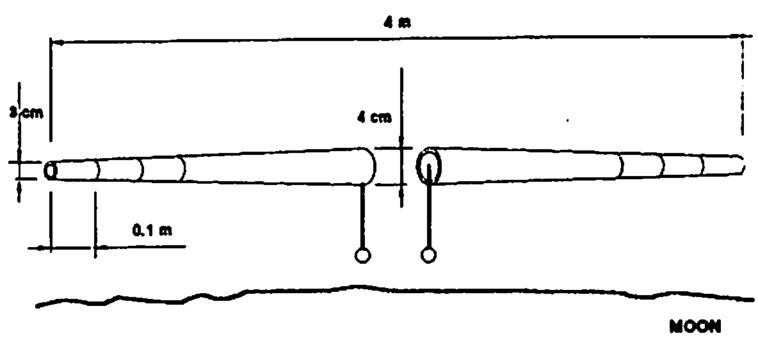

Fig. 6.5 Dipole dimensions

Due to the impedance matching characteristics of a short dipole, it is extremely difficult to achieve good matching with a passive network. Thus an active matching solution using FETs was used. The radiation performance of the proposed dipole is shown in Figure 6.6and is quasi independent of frequency. Only at zenith is a perfect circular polarisation obtained. However, up to zenith angles of about 50°, the level of circular polarisation is good (~ 3dB drop in axial ratio). The effect of a real ground plane close to the dipole has been simulated using image theory and Fresnel reflection coefficients. For the moon soil it has been assumed $\epsilon_r = 3$ and $\sigma = 10^{-4}$ mho/m. The effect of the ground is to reduce the lobe pointing towards the sky and to correspondingly increase the one pointing towards the moon, thus introducing losses around 3 dB. A typical situation is depicted in Figure 6.6. The influence of the ground on the input impedance and the effective area are very much dependant on the actual conditions on the moon and should be investigated as part of the precursor missions.

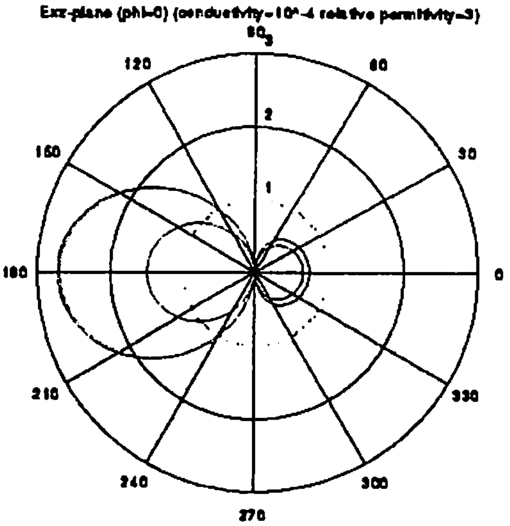

Fig. 6.6 Cross section of the radiation pattern perpendicular to the dipole. The circle of radius 1 corresponds to the dipole in free-space while the lobes represent the pattern on the moon surface. The inner trace corresponds to 500 kHz and the outer one to frequencies between 5 and 15 MHz.

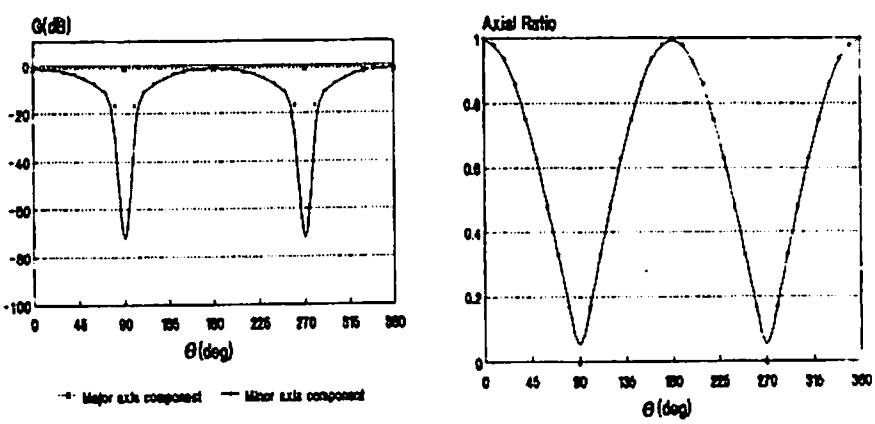

Fig. 6.7 Cross section of the radiation pattern of the dipole. The major axis is the horizontal field component, and the minor axis is the vertical field component.

6.4.2 Radio receiver module

The radio receivers are very simple. Figure 6.8shows the diagram of the basic electronic system. It is composed of two super-heterodyne receivers, one for each polarisation, operating in the 0.5-16 MHz range. Two intermediate frequencies (IF) are used, the first one at 38.9 MHz, and the second at 455 kHz. The analog signals are then digitised at 200 kHz, the Nyquist rate, and modulated using four level phase shift keying (4-PSK) for transmission to the central station.

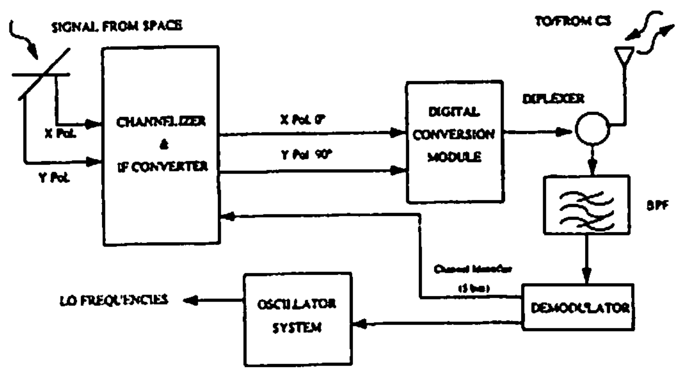

Fig. 6.8 General receiver element block diagram.

A local oscillator generates all frequencies and phase references for the conversion sampling and modulation stages, and to synchronise all oscillators to that of the control station. The frequency allocation of the base-band signal from each receiver element is shown in Figure 6.9.

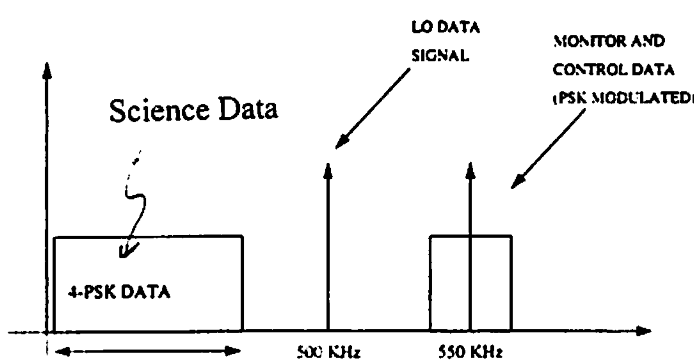

Fig. 6.9 Baseband signal from the receiver.

6.4.3 Power subsystem

Each receiver is an autonomous element which needs power for sky signal reception, internal signal processing, RF link with the Central Station, and thermal control. Receivers are operated only during night, and the total continuous power required is estimated at 2 Watts, broken down as indicated in Table 6.3. This is supplied by a battery which is recharged by a solar panel during lunar day.

Discounting solar power when the sun is below 10 degrees above the horizon, the battery must be able to supply power for about 15.6 earth days or 370 hours per lunar day cycle, i.e. a total of 740 Wh. Because of the strong mass limitations of lunar missions, we have selected a lithium-thionyl chloride battery which offers a very high power density (500 Wh/kg) and high cell voltage (3.3 V). An example of such battery is produced commercially for telecommunication purposes by SAFT. They are extremely safe and reliable and have a lifetime of 5 to 7 years. They must be used in the 30 to 70 °C temperature range, the optimum capacity is obtained at 70 degrees and is reduced by 50 % at 40 degrees C.

Allowing a battery efficiency of 90% and a 90% depth of discharge at the end of night, the battery must have a capacity of:

$$\frac{740\mathrm{Wh}}{3\mathrm{V} \times 0.90 \times 0.90} = 300\mathrm{Ah} \tag{6.8}$$

which entails a battery mass of about 1.8 kg.

Now, assuming a battery efficiency of 90% and a charge efficiency of 95% the battery charging power to be supplied during the lunar day by the solar panel will be $740/(0.90 \times 0.95) = 868\mathrm{Wh}$, and its average generated power at end of life must be 868Wh/302=2.87 Watts. The solar panels use GaAs cells which have a high efficiency and generate 220 mA at 0.87 V under normal incidence and at the estimated operating temperature of 110 °C. These figures includes a 5% allowance for degradation at end of life.

Integrating the solar flux over the lunar day for the site latitude selected, the required solar panel area is 290 cm^2. The cells are mounted on a 20 cm × 20 cm honeycomb panel leaving space for wiring and blocking diode. The estimated mass is 250 grams.

The power subsystem also includes a battery charge regulator and a power distribution unit of conventional design. These can be manufactured in VLSI in a single chip, so that the mass of the power subsystem electronics can be as low as 50 grams.

6.4.4 Packaging

The receiving element is shown Figure 6.10. The main box structure is 250 mm × 250 mm × 250 mm, and is composed of an aluminium frame and carbon fibre sandwich panels. Each dipole boom is 2 meter long and composed of 12 telescopic elements about 40 mm in diameter and 0.2 mm thick. The dipole antenna booms are deployed by simple spring loaded mechanisms mounted on the box corner ribs. Alternatively, the dipole booms could be composed of a circular section tape deployed from a small cassette drum. The estimated mass of the receiving module is shown in table 6.3. The horn antenna is mounted on an articulated arm which is deployed automatically. The horn must be oriented within 10 degrees of the direction to the central station; this direction is preset for each receiver dependent on its predicted location in the array.

Table 6.3 Receiving element mass and power

Item	Mass (kg)	Power (Watts)
Box	0.58	-
Horn antenna and mechanism	0.50	-
Battery	1.80	-
Electronics	0.30	0.5
Dipole	0.85	-
RF link	-	0.5
Thermal control	0.16	1.0
Solar panel	0.25	-
Contingency	0.43	-
Total	4.88	2.0

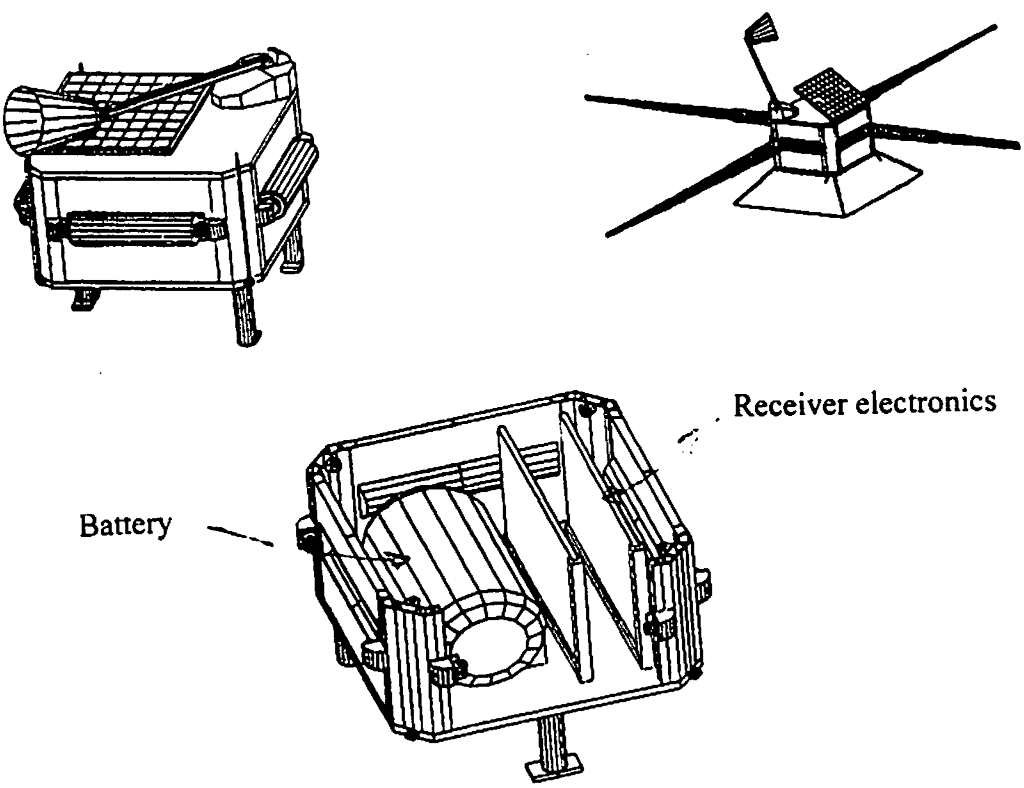

Fig. 6.10 An individual receiving module shown stowed for launch (top left) and deployed (top right). The cutaway view at bottom shows the inside packaging.

6.4.5 Thermal control

At the low latitude of the selected site (Tsiolkovsky crater, 20 °S) the day/night temperature swing is extreme, with a maximum temperature close to 135 °C and a minimum temperature during night time between -200 and

-150°C.

The electronics can be safely operated in a -20 and 60 °C temperature range, and the Lithium-thionyl chloride battery has its better performance at 70 °C. Since the heat sources are very low (both the battery and electronics dissipate very little power, 1 Watt total), the receiving element will be essentially isothermal. Thermal modelling has shown that the optimum operating temperature is around 40 °C, an operating point where the battery efficiency is still good, and the night time heater power consumption reasonable (1 Watt). The box is wrapped with a thermal multi-layer insulation to minimise conduction and radiation with the lunar soil and to reflect sunlight during the day. In addition the receiver box is surrounded with a Teflon foil skirt to shade the moon surface from the sun near element in order to reduce conduction and radiation losses. The thermal-optical properties of the receiver module materials and of the moon soil are given in Table 6.4.

Table 6.4 Thermo-optical properties

Material	Absortivity (α)	Emissivity (ϵ)
MLI external layer (silvered Teflon) 0.15	0.61	
Teflon Foil external panels	0.15	0.61
Solar panel	0.72	0.83
Moon surface	0.93	1.0

6.5. Solar system receiver

The need for that instrument arises from the possibility to disentangle the solar contribution from the extra-solar signal received, but it can be used in its own right to perform solar system science.

Since the location of the solar system sources are well known, there is no need for spatial resolution and it is possible to use a single radiometer connected to an omni-directional antenna.

6.6. Central station

The central station performs all data handling, monitoring, telemetry and telecommand function tasks for the entire array. It also serves as a control centre during the robotic deployment of the receiver elements. It is mounted on the moon lander with solar panel, radiator and antenna deployed upon landing (Figure 6.11). The two large boxes on the lander contain the receiver elements which are extracted by the robotic rover using an access ramp. The fuel tanks are thermally insulated with MLI following landing and vented.

The antenna for data interchange with the receiver elements is a simple omni-directional conical antenna on a 9 meter mast via the antenna for the satellite link is a conventional 0.5 meter dish with tracking capability to follow the satellite in its halo orbit. A pair of crossed dipoles, identical to those of the receiver elements, is also located on the central station for array calibration purposes.

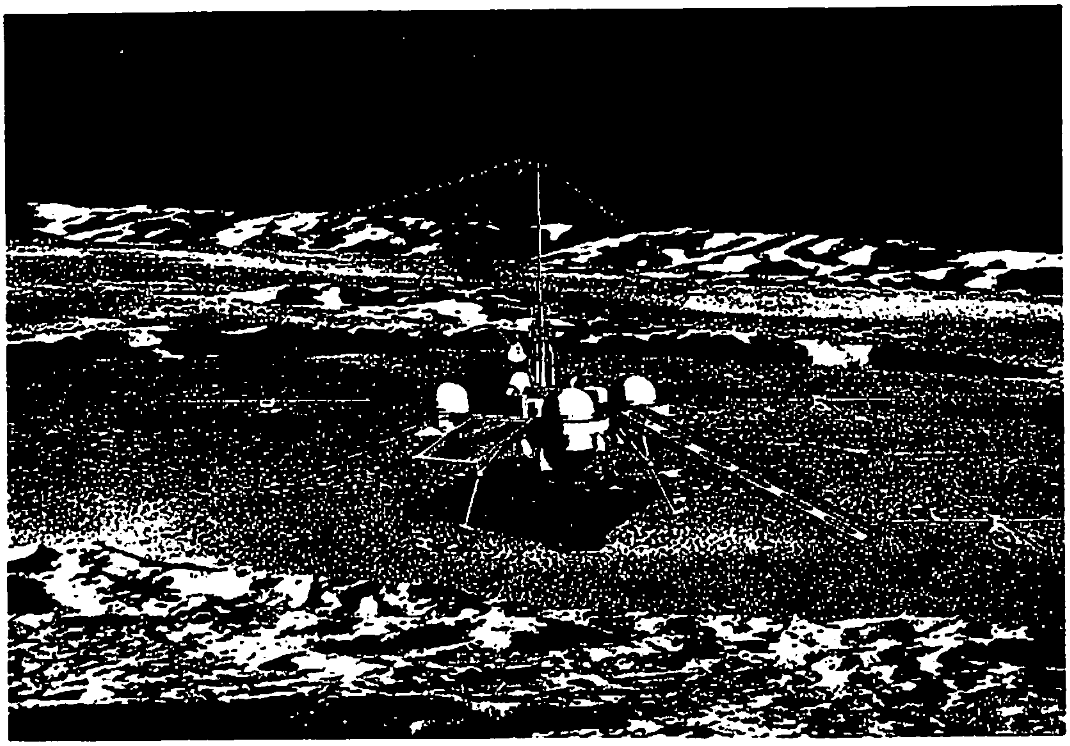

Fig. 6.11 General view of the central station.

The power required during lunar night, estimated at 200 W, is supplied by a lithium thyonil-chloride battery recharged by a solar panel during lunar day.

The basic block diagram of the correlating system is shown in Figure 6.12. The system outputs the visibility function for each pair of array elements. Post correlation reconstruction of the source brightness distribution is done on earth.

6.7. Site selection

The array should be located beyond 30 degrees from the moon limb in order for the earth radio interference to be negligible. Another condition is that it be situated near the equatorial plane for practically full sky coverage. Another advantage of an equatorial location is that it minimizes the orbital transfer energy which permits a larger payload mass.

From the topographical point of view, the area selected must be quite flat in order to permit direct line of sight between the central station and the receiving element or repeaters for communication link. Candidate sites are shown in Table 6.5.

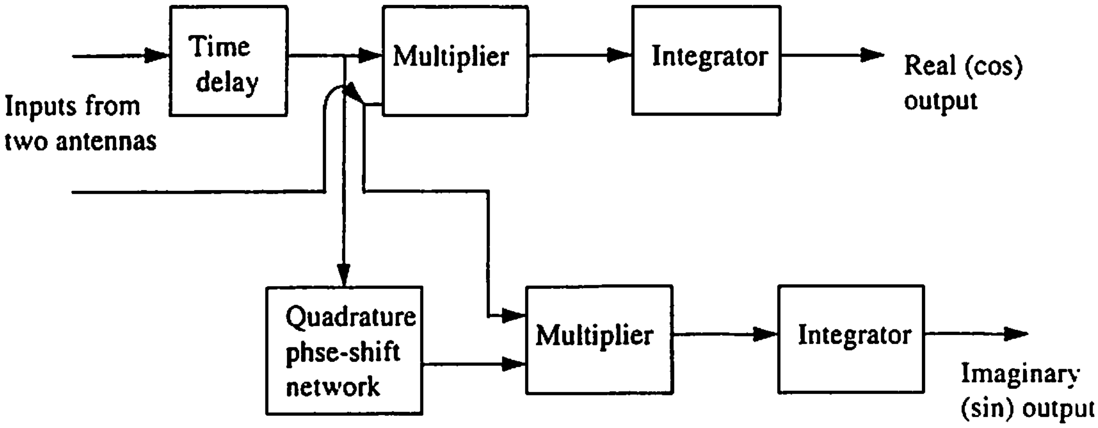

Fig. 6.12 Block diagram of the correlation system

Table 6.5 Candidate sites

Crater	Coordinates	Diameter (km)
Aitken	17°S, 173°E	50
Isaev	17 °S,148 °E	25
Kohishutter	27°N, 154°E	25
Langemak	10°S, 119°E	<25
Tsiolkovsky	20°S, 129°E	100

In the selected spiral array configuration, the maximum distance between the central station and the receiving element is about 70 km. The only large enough flat area to be found near the equator and 30 degrees from the limb is the Tsiolkovsky crater. The Tsiolkovsky crater is filled with a mare with a particular dark colour, but the exact topography is not known.

The magnetic field in the Tsiolkovsky area is lower than average, which is favourable from the point of view of ionospheric effects.

References and bibliography

G.J. Burke, "Recent advances to NEC: Applications and validation". Agard lecture series No. 165.

W.N. Christiansen, J.A. Hogbem, "Radiotelescopes", Cambridge University Press, 1969.

M.P.M. Hall, L.W.Barclay, "Radiowave propagation". Peter Peregrinus Ltd. 1989.

Heiken, G.H., Vaniman, D.T. & Bevan, M.F., "The lunar source book". Cambridge University Press. 1991.

L. J. Chu. "Physical limitations of omnidirectional antennas". J. Appl. Phys., vol.19, pp 1163-1175, Dec. 1948.

H. Jasik, "Antenna engineering handbook", McGraw-Hill, 1961.

H.L. Krauss, C.W.Bostian, F.H.Raab, "Solid-state radio engineering", New York. Wiley, 1980.

Y.T. Lo, S.W. Lee, "Antenna Handbook. Antenna fundamentals and mathematical techniques". Vol. I.. 1993.

H. Mott, ""polarisation in antennas and radar". John Wiley & Sons. 1986.

P.J. Napier, A.R. Thompson, R.D. Ekers, "The Very Large Array: design and performance of a modern synthesis radio telescope" Proc. of the IEEE, vol. 71, 11, Nov. 1983.

P.J. Napier et al. , "The Very Long Baseline Array": Proc. of the IEEE, vol. 82, 5, May 1994.

H.S. Rauschenbach, "Solar Cell Array Design Handbook", 1980.

U.L. Rohde, T.T.N. Bucher, "Communications receivers. Principles and design", New York. McGraw Hill. 1988.

Rohde, Schwartz, "Communications receivers. Principles and design".

R. A. Sainati and D.E. Fessenden. "Performance of an electrically small antenna amplifier circuit". IEEE Trans. on aerospace and electronic systems, vol. AES-17, No.1, pp. 88-92, January 1981.

P.N. Slater, A.K.Fung, "Microwave remote sensing vol. I ", Addison-Wesley. 1982.

W.L.Stutzman, G.A.Thiele, "Antenna theory and design". John Wiley & Sons. 1981.

A.R. Thompson, J.M. Moran, G.W. Swenson. Krieger, "Interferometry and synthesis in radio astronomy", 1994.

R. N. Velev and R. W. King. "An active antenna for TV Bands 3,4 and 5".

7

LAUNCH AND DEPLOYMENT

The total mass of the 300 receiver elements is 1320 kg and the central station mass is estimated at 200 kg, including storage boxes for the receiving elements. Although the design of a moon lander was not part of this study, its mass can be estimated at 1200 kg so that the total mass to be delivered to the moon is 2720 kg which is within the capability of a single Ariane 5E launch.

This approach takes into account that precursor missions will have brought a rover that can be used for the deployment of the receiver elements, and that a communication satellite at the L2 point will also be in place.

Following landing on the moon surface, the central station is activated for monitoring the receiver elements deployment and perform functional checkouts as they are installed. The 100 receiving elements of a given branch of the array are contained in a single carriage on the lander. The rover takes one of these carriage in tow and disposes the individual receiver elements at their assigned location along the spiral arm of the array.

Each spiral arm is 80 km in length. Assuming a rover speed of 2 km/h and 30 minutes for each receiver element installation, the deployment of the 3 arms of the array will take approximately 270 hours ($\sim$ 12 earth days) and would thus fit within one lunar day.

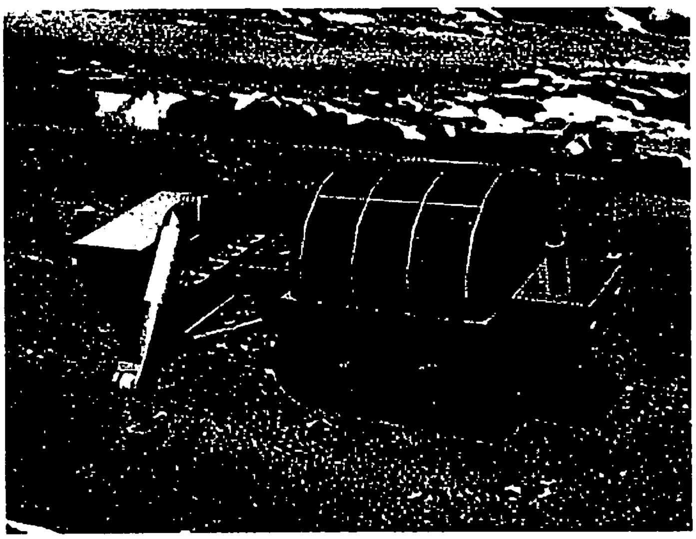

Fig. 7.1 Artist's concept of the robotic deployment

References

"Performance Ariane 5 en mission lunaire", J. Ciampi. CNES. 27/07/93 "Fundamentals of Astrodynamics" Bate, Mueller, White. Dover. 1971

8

COST ESTIMATE

Table 8.1 Payload cost estimate (MAU's)

Item	MAU's	
Array receiver element		
Design and Qualification	40	
Manufacturing (300 units at 0.16 each)	50	
Total receiving elements (300)		90
Repeaters		
Design and qualification	4.5	
Manufacturing (9 at 0.5 each)	4.5	
2.25 Total Repeaters (9)		9
Central Station		
Design and Qualification	10	
Manufacturing	20	
Total Central station		30
Contingency		21
Total payload	150 MAU	

The total cost of the mission will greatly depend on the availability of a rover, lander and relay satellite from other moon programs . In the event where a rover, basic lander and relay satellite exist, a rough order of magnitude cost of the VLFA mission would be about 520 MAUs broken down as is shown in Table 8.2

Table 8.2 Mission ROM cost

Item	MAU's
VLFA payload	150
Ariane 5 launch	120
Basic moon lander	Not incl.
Lander modification	150
Rover	Not incl.
Ground Segment	100
Total	520 MAU

9

PRECURSOR MISSION

A number of questions need resolving before the start of development of the VLFA. Some of these questions can only be resolved by performing measurements in the vicinity of, or on the moon. The main questions are listed below:

Ionospheric survey of moon environment. The design and performance prediction of the VLFA makes the assumption that the local ionosphere of the moon does not substantially limit the performance. This must be verified by demonstration at the earliest opportunity. Active sounding either from lunar orbit or from the lunar surface is required.

Electrical properties of the lunar surface. The electrical properties of the lunar surface that have most influence on the shape of the beam of a single antenna are the electrical permittivity and electrical conductivity. These have been measured during the Apollo mission. More extensive measurements need to be made to ensure we have a full range of measurements covering all candidate sites for the VLFA. We must also understand the variation of properties as a function of depth as at these wavelengths the properties down to several meters will determine the beam shape. Such measurements may be performed by an orbiting satellite and by in situ measurements.

Electrical survey of candidate site. Although the antenna gain is higher in the direction into the lunar surface the contribution to the noise figure from this source is low as the moon is cold in comparison to the sky. This is only true if there are no reflections of the sky into the lunar surface pointing lobe of the antenna from discontinuities in electrical properties within several wavelengths of the surface. A detailed sounding of the candidate site is therefore required. This is best performed by surface measurements.

Topological survey of candidate sites. To establish the possibility of line of site connection between the receiver elements and the central station or relay stations, a topological survey to an accuracy of 0.5 meters or better in altitude over a grid size of 10 meters is needed. It is hoped that a site could be found which would not require relay stations. Such a survey can best be performed by an orbiting satellite using laser or radar sounding together with high resolution imaging.

Magnetic survey of candidate sites. To establish any effects due to interaction with the local plasma, a site with low magnetic field is required. A magnetic survey from an orbiting satellite will be required first, followed by magnetic measurements on the surface.

Verification of Earth noise attenuation. The siting of the VLFA on the lunar far side, at least 30 degrees from the limb, is dictated by the need for adequate attenuation of both man made and natural emissions from Earth and its environment. Initial measurements can be made from an orbiting satellite and later verified on the lunar surface.

The following is a proposal on how the above objectives can be achieved in the phases leading up to the VLFA deployment in a timely manner.

Phase 1 precursor activities: There are two ESA candidate missions for Phase 1 of the ESA moon initiative namely MORO, a scientific mission for a polar orbiting satellite, and LEDA a technology mission to land a rover and small science package close to the southern pole of the moon. MORO is proposed to have an altimeter and imager capable which will satisfy the major objectives of topological survey of candidate sites for the VLFA

The LEDA mission will allow the deployment of a simple two element interferometer, one element situated on the lander and the second element on the rover. By observing Earth based transmissions, the performance impacts due to any local ionospheric effects can be verified. Additionally active sounding can be used to probe the ionosphere and the local subsurface. Such an instrument should not weigh more than 1 Kg.

The NASA mission Lunar Prospector will also provide data on the lunar magnetic environment.

Phase 2 precursor activities: Surface exploration of the total moon surface is one objective of phase 2. This will require the development of high performance landers, rovers and robotic manipulators as well as a relay system to support the exploration of the lunar far side. The development of these facilities could take into account the requirements of the VLFA in order to allow a timely deployment of this facility in phase 3.

10

CONCLUSION

This study has confirmed that observations in the frequency band 500kHz to 16 MHz can be made with a simple equipment placed on the far side of the Moon. These observations cannot be performed from the Earth's surface, due to the ionospheric cut-off, or from an Earth orbit because of man-made and ionospheric noise. The lunar near-side would also suffer from interference. Within our solar system neighbourhood, only the Lunar far-side, using the Moon as a shield from Earth emitted radiation, will allow these very low frequency observations.

Although no observations with a resolution better than 60 degrees have been performed at frequencies below 1MHz, we can theorize on the nature of the observable sky in this spectral band. We find that the sky will be bright but with little fine structure due to strong scattering by the interstellar and interplanetary media. Interplanetary scattering dominates over the interstellar, being 100 arcminutes at 1 MHz compared to 22 arcminutes for interstellar. We also expect that there will be temporal broadening and Faraday depolarisations. Measurements in this band should reveal as much about the intervening medium as about the sources generating the signal. For this reason the primary science objective will be to perform an all sky survey with a resolution of 0.5 degree at 1 MHz. The survey will be conducted in narrow bandwidths of 100 kHz. This survey can be completed in the expected 5 year mission lifetime. In addition, a receiver system with little directional resolution will monitor objects within the solar system.

A spatial resolution of 0.5 degrees at 1 MHz requires a baseline of 40 km. Achieving the sensitivity requirement requires 300 separate antennas. The antennas are distributed over a three-arm spiral and maintain a reasonably constant signal to noise ratio over the full frequency band of 500 kHz to 16 MHz.

The individual receiver elements are simple crossed dipoles lying on the lunar surface. As observations will have to be performed during the lunar night to avoid the moon's ionospheric cutoff, each receiver element contains a battery which is recharged by a solar array. Data will be collected from the central station by a relay satellite in halo orbit at about the L2 point of the Earth-Moon system. The 300 receiving elements and central station are within the payload capacity of a single Ariane 5 launch. Deployment of the receiving antennas will be performed robotically by rover.

A number of assumptions have been made in establishing the design of this VLFA array, in particular concerning the characteristics of the moon's ionosphere. These assumptions should be verified during earlier missions such as MORO and LEDA.

This study has shown the scientific interest of this unexplored region of the electromagnetic spectrum. The technical implementation is within the present state of the art. The deployment of the array seems ideally compatible with the objectives defined for Phase 3 of the proposed ESA Lunar Programme.

Appendix A
Study participants

Roberto Ambrisoni
Radioastronomer
Tel: (39) 51 6399361
Fax: (39) 51 6399431
e-mail:ambrosini@astbo1.bo.cnr.it

Arnold von Ardenne
Radioastronomer
P.O. Box2
7990 AA Dwingeloo
The Netherlands
Tel: (31) 521 595134
Fax: (31) 521 597332
e-mail:ardenne@nfra.nl

Colin H. Barrow
Radioastronomer
Max-Planck-Institut für Aeronomie,
D-37189 Katlenburg-Lindau, Germany
Tel: (49) 5556 979156
Fax: (49) 5556 979240
e-mail: barrow@linax2.dnet.gwd.de

Pierre Y. Bély
Chief Engineer
Space Telescope Science Institute
3700 San Martin Drive
Baltimore, MD 21218, USA
Tel: 410 338 4780
Fax: 410 338 1592
e-mail:bely@stsci.edu

Jean Louis Bougeret
Radioastronomer
DESPA, URA CNRS 264
Observatoire de Paris-Meudon
92195 Cedex, France
Tel: 33 (0)1 45 07 77 04
Fax: 33 (0)1 45 07 28 06
e-mail:bougeret@obspm.fr

Robin Laurance
Future Science Projects Office
ESA/ESTEC
Postbus 299
2200 AG Noordwijk zh
The Netherlands
Tel: (31) 71 565 3516
FAX: (31) 71 565 5417
e-mail:rlauranc@estec.esa.nl

Juan-Maria Marcaide
Professor of Astronomy
Dpto. de Astronomia
46100 Burjassot-Valencia
Spain
Tel: (34) 6 386 4549
Fax: (34) 6 386 4364
e-mail:jmm@vlbi.matapl.uv.es

Felix Lamela
Analysis engineer
CASA Space Division
Avda de Aragon 404
28022 Madrid Spain
Tel: 34 1 586 3798
Fax: 34 1 586 4799
e-mail:

Fernando Monjas
Telecommunication engineer
CASA Space Division
Avda de Aragon 404
28022 Madrid Spain
Tel: 34 1 585 77 12
Fax: 34 1 747 47 99

Enrique Rey
Telecommunication engineer
CASA Space Division
Avda de Aragon 404
28022 Madrid Spain
Tel: 34 1 586 7820
Fax: 34 1 747 47 99
e-mail:

Sergio Volonte
ESA Headquarters
8, rue Mario-Nikis
75738 Paris Cedex 15
France
Tel: 33 (0)1 53 69 71 03
FAX: 33 (0)1 53 69 72 36
e-mail:svolonte@esa.bitnet

Kees van't Klooster
Electromagnetics Division
ESA/ESTEC
ph: 31 71 565 3940
fax: 31 71 565 4999
email: kvtkloos@estec.esa.nl

Graham Woan
Lecturer
Department of Physics and Astronomy,
University of Glasgow,
Glasgow, G12 8QQ, UK
tel: 44 141 330 5897
fax: 44 141 330 5183
e-mail:graham@astro.gla.ac.uk